The Static Universe Hypothesis:
Theoretical Basis
and
Observational Tests of the Hypothesis

Thomas B. ANDREWS

(tom-andrews@msn.com)

September 6, 2001

Abstract

From the axiom of the unrestricted repeatability of all experiments, Bondi and Gold (also Hoyle) argued that the universe is in a stable, self-perpetuating equilibrium state. Their reasoning extends the usual cosmological principle to the perfect cosmological principle in which the universe looks the same from any location at any time. By itself, the perfect cosmological principle predicts the universe is static and in an equilibrium state.

However, Bondi and Gold rejected the static universe prediction for two reasons: First, they believed the universe was expanding because of the Hubble redshift. Second, the universe appeared to be far from thermodynamic equilibrium. Therefore, they hypothesized that the universe was expanding and in a steady-state. The steady-state universe is an expanding universe model in which matter is created. As the galaxies recede, new galaxies form from the created matter and maintain the universe in a stationary state.

Instead of the steady-state model or the current Friedmann-Walker expanding universe model, I hypothesize that the universe is static and in an equilibrium state (non-evolving) as predicted by the perfect cosmological principle.

New physics is proposed based on the concept that the universe is a pure wave system. Based on the new physics and assuming a static universe, new processes are derived for the Hubble redshift and the cosmic background radiation field.

A new time-dilation process is proposed as the cause of the anomalous dimming of Type Ia supernovae at high z. This process is based on the Hubble redshift increasing the period of the supernovae luminosity curve in the observer's rest frame. In turn, the increase in the period reduces the luminosity of supernovae by $1/(1+z)$. Furthermore, since this process is independent of the cause of the Hubble redshift, the new time-dilation

1

process must also apply to supernovae in the expanding universe models. But, the expanding universe model already incorporates a time-dilation effect which applies to any object. Thus, two time-dilation effects should be observed for supernovae. Since only one time-dilation effect is observed for supernovae, the expanding universe model is logically falsified.

Following the scientific method, I test deductions developed from the static universe hypothesis using observational data primarily from the Hubble Space Telescope. Applying four different global tests of the space-time metric, I find that the observational data consistently fits the static universe model and, therefore, confirms the static universe hypothesis. The observational data also show that the average absolute magnitudes and physical radii of first-rank elliptical galaxies have not changed over the last 5 to 10 billion years, thereby confirming the perfect cosmological principle.

In the expanding universe models, the observed baryonic mass density is a factor of 25 to 50 lower than the predicted mass density in a flat universe. This discrepancy between theory and observation is a major problem and has resulted in many hypotheses concerning the nature of the "missing mass." In the static universe model, the predicted baryonic mass density is lower by a factor of about 20. Consequently, the discrepancy in the baryonic mass density between theory and observation is removed.

Because the static universe hypothesis is a logical deduction from the perfect cosmological principle and the hypothesis is confirmed by the observational data, I conclude that the universe is static and in an equilibrium state.

Contents

1   Introduction

The current standard model of the universe is the Friedmann-Walker expanding universe. The major factors which led to the adoption of the expanding universe model in the late 1920's and early 1930's were:

1. The distribution of the galaxies is homogeneous and isotropic.

2. The galaxies are receding from us with velocities proportional to their distances.

The first factor is undoubtedly correct. Observations show that the galaxies on a large enough scale are distributed homogeneously and isotropically. However, the recession of the galaxies was based on the Hubble redshift which remains an assumption. Initially, the redshift was assumed due to the Doppler shift process and, later, to the expansion of space. Thus, the Hubble redshift could still be due to a different process.

If another process is responsible for the Hubble redshift, the theoretical picture becomes quite different. The universe would be static rather than expanding. This, of course, is only a conjecture at this point but it is an important first step.

A few cosmologists, notably Jaakkola [1] and LaViolette [2], have proposed that the universe is static. Jaakkola has argued that the universe is static and in an equilibrium state. LaViolette has shown that the observational data of the mid-1980's is more consistent with the static universe model than the expanding universe models and proposed a new process for the Hubble redshift. I also proposed [3] that the universe was static in 1994. However, at that time, the observational data was not good enough to convincingly prove that the universe was static. On the other hand, Sandage and Lubin [4] have recently concluded from surface brightness observations of elliptical galaxies that the universe is expanding.

This paper is equally divided between theory and observation. The theoretical part is required to derive the Hubble redshift and predict the mass density of the universe. The observational section is also large in order to adequately describe and analyze the observational data sets. Consequently, the paper is organized as follows:

1. The static universe hypothesis is developed. This is an important first step in the scientific method [6].

2. New physics is introduced in order to derive the Hubble redshift. New physics in this instance appears required since all previous attempts to derive the Hubble redshift using current physics appear to have failed.

3. The source of the mass-energy of elementary particles is determined. In particular, an average mass density of the universe consistent with observation is predicted.

4. The size and physical nature of the universe are discussed. This section contains another argument for a static and equilibrium universe.

5. A new Hubble redshift process is derived for a static universe. This process applies to both photons and mass particles.

6. A theoretical solution to the anomalous dimming of supernovae is proposed based on a new process involving time-dilation of the supernovae light curve.

7. An equilibrium energy process is proposed for the Cosmic Microwave Background (CMB) radiation field in a static universe.

8. The deductions of the static universe hypothesis are compared to the observations, using four different global tests of the space-time metric.

2   The Static Universe Hypothesis

Rather than argue for a static universe hypothesis as in the introduction, it is better to develop the hypothesis based on physical logic. Thus, the hypothesis of a static universe in an equilibrium state follows directly from the perfect cosmological principle (PCP) which was proposed in 1948 by Bondi and Gold [7] (also Hoyle [8]). The PCP says the universe looks the same from any location at any time.

Bondi and Gold based the reality of the PCP on the following fundamental assumption:

> Given that the unrestricted repeatability of all experiments is a fundamental axiom of physical science, this implies that the outcome of an experiment is not affected by the location and time at which it is carried out.

They believed that cosmology must be concerned with this fundamental assumption and, in turn, an adopted cosmology must incorporate this assumption.

Based upon this fundamental assumption, Bondi and Gold then developed the following paradigm:

> As the physical laws cannot be assumed independent of the structure of the universe and, conversely, the structure of the universe depends upon the physical laws, it follows that the universe is in a stable self-perpetuating state, without making any assumptions regarding the particular features which lead to this stability.

They emphasized that only in such an equilibrium universe can the constants and laws of physics be invariant to both changes in location and time.

Of course, Bondi and Gold did not absolutely claim that the PCP must be true. However, they believed that if it does not hold, the variability of the physical laws becomes so wide that one can no longer use local physics in the

distant universe without relying on arbitrary principles for the extrapolation of local physics.

Conversely, if the PCP holds in the universe, we can confidently base our results on the permanent validity of all our experiments and observations. Therefore, they concluded that we should proceed theoretically assuming the PCP is true since this is the only basis permitting progress without further arbitrary assumptions.

At the present time, the PCP must be considered an even stronger theoretical principle since the invariance of the physical constants [9] and the laws of physics are confirmed both by local experiments and by distant observations of the universe.

From the PCP, Bondi and Gold at first expected the universe to be static. However, because of the observed redshifts of the galaxies and also the active state of universe, they believed the universe must be expanding and thermodynamically in a non-equilibrium state. Then, in order to maintain a stationary state of the universe even though the universe was expanding, they were forced to assume that matter is created in the voids left by the expansion of the space between the galaxies. They referred to this new model of the universe as the steady state universe.

From today's perspective, I believe their initial expectation that the universe was static was correct but that their further assumptions leading to an expanding universe with matter creation were both unnecessary and incorrect. However, in 1948 when they developed the PCP, the steady state universe was possibly the only logical way to proceed.

Currently, based on the derivation of a new process for the Hubble redshift in a static universe, many of the elements of a static universe are understood. In any case, the static universe hypothesis can now be tested since precision observational data is now available from the Hubble Space Telescope and the new, large ground telescopes.

3 New Physics

The basic problem is to develop a new process for the Hubble redshift in a static universe. Since the Hubble redshift has been known for over 70 years, a large number of attempts have been made to derive a physical process for the Hubble redshift in a static universe. The requirements for the Hubble redshift process are:

1. The shift in frequency is strictly proportional to the frequency.

2. All electromagnetic frequencies are equally affected.

3. The redshift is proportional to the distance.

The first two requirements are satisfied by the Doppler process but, of course, it is not the Doppler process which is now held responsible for the redshift but the expansion of the universe. The expansion fits all of the above requirements.

Gravitation is the only other known process with the same properties. So, without introducing a new force, gravitation is an obvious candidate for the Hubble redshift. However, in current physics, gravitation is too weak a force to cause the Hubble redshift. This is the current dilemma if new physics is not introduced.

3.1 The Wave System Theory

As a more fundamental and comprehensive viewpoint in physics, I propose *the Universe is a Pure Wave System consisting of a large number of wave modes.* This is a new paradigm that was inferred from the universal occurrence of wave phenomena in physics and the consistency of the paradigm with the basic laws of physics. From this concept of a wave system, the existence of particles, fields and quantum effects [10] may be derived.

Because the wave modes have very small amplitudes, I assume the wave modes can be modeled using the classical linear wave equation

$$\frac{\partial}{\partial x}\left(T(x)\frac{\partial \phi}{\partial x}\right) = \sigma(x)\frac{\partial^2 \phi}{\partial t^2} \tag{1}$$

where the parameters, $T(x)$ and $\sigma(x)$, are the tension and (linear) mass density respectively. The parameters are not fixed but can vary subject to local constraints. And, because the parameters can vary, the wave modes can exchange energy through parametric interactions.

The wave modes can be shown to constructively interfere and produce localized peaks surrounded by large regions of destructive interference. It is then hypothesized that these localized peaks are the elementary particles. As derived later, the wave system becomes a deeply bound system when the localized peaks are formed. The system then appears to consist only of stable, interacting constructive interference peaks, indistinguishable in properties from the observed elementary particles.

A symmetry argument of H. Giorgi [11] proves that the wave system exists. Given a system which is infinite and linear and where the laws of physics are space and time translation invariant, Giorgi argues that the modes of oscillation of a system are determined by the representations of the space and time translation groups. Since a solution of each representation is a complex exponential in space and time respectively, a standing wave system is formed, given by $\exp i(\omega t \pm kx)$.

The symmetry proof must apply to the universe since the properties of the universe match very closely the requirements for the symmetry. First, the universe is a very large if not infinite system with linear responses at the level of basic laws. And second, the exact time and translational invariance of the laws of nature has been experimentally confirmed.

C. Vassallo [12] reaches similar conclusions. He also finds that fields which are invariant to space and time translation must vary as $\exp i(\omega t \pm kx)$. In addition, he finds that any bounded wave field which has sources can be represented

8

by normal modes which do not have sources. This is a significant theorem. It suggests that a system of bounded normal modes can bootstrap initial sources to produce the normal modes.

The stability of the wave system is based on the following two principles:

1. The frequency is reduced if the mass density and tension are larger at the wave mode peaks.

2. As the number of elementary particles mutually interacting increases, the frequency increases.

To apply the first principle, assume the mass density and tension are proportional to the local energy density of the wave system. Then, the frequency of a wave mode will decrease when the constructive interference of the wave modes produces high energy concentrations at the peaks of the wave mode (See equation 9 and accompanying discussion). As an example of this principle, consider a string vibrating in it's lowest frequency mode. When lead weights are placed at the peaks of the vibration, the frequency is reduced. Similarly, when the tension is increased at the peaks, the frequency is reduced. Since the energy density at a peak is proportional to the number of wave modes ($N \approx 10^{38}$) constructively interfering, the decrease in frequency of the wave modes is very large. If the natural frequency of the wave system without constructive interference is f_o, complete constructive interference reduces the frequency to

$$f_m = \frac{f_o}{\sqrt{N}}. \tag{2}$$

Since the number of wave modes increases as the average distance between particles increases, the frequency could go to zero as N increases without limit. However, by the second principle, there is a lower bound on the frequency determined by the number of interacting particles in the universe. This frequency is given by the simple eigenvalue equation proposed by Chen [13]

$$f_p = \frac{1}{2\pi}\sqrt{n}\sqrt{k/m} \tag{3}$$

where n is the effective number of particles interacting and the interaction constant, k/m, between any two particles is constant.

This eigenvalue system is remarkable since it has only two discrete frequencies, one degenerate with $n-1$ modes given by f_p and the other equal to $f_o = f_p/\sqrt{n}$, the frequency of a single element and also the minimum frequency. Equation 3 is the approximate eigenvalue solution to the interactions between all the particles ($\approx 10^{80}$) in the universe. This assumes that in the universe the interactions between particles have the same average strength.

A stable frequency of the wave system is attained when the wave mode frequency, f_m, and the particle frequency, f_p, are the same. The particle frequency may be estimated from equation 3. Let $f_o = 1/(2\pi)\sqrt{k/m} = c/(2R)$. R is the mean absorption distance and is equal to c/H (see section 5). $c/(2R)$ estimates

9

the minimum frequency, f_o. Then, assuming $R = 1.85 \times 10^{28}$ cm (H = 50 km/sec/Mpc) and $n \approx 10^{80}$ particles, the stable frequency is 8.1×10^{21} Hertz.

As a first approximation, the wave system vibrates at this single frequency. In the second approximation, the single frequency is split into two frequencies by the interactions between the particles. The higher frequency is hypothesized to correspond to the proton and the lower frequency to the electron. This eigenvalue theory is consistent with the fact that these are the only stable mass particles.

The number of normal modes is an important parameter in the wave system theory because the properties of the wave system depend on constructive interference. In particular, the ratio between the electrostatic force and the gravitational force is proportional to the number of modes interfering. This can be shown as follows: For constructive interference, the intensity, I, at a particle is proportional to

$$I \propto \sum (A_1 + A_2 \ ... \ A_N)^2 = NA^2 \pm 2N^2A^2 \tag{4}$$

where A is the amplitude of each mode of vibration. It is assumed that the force of gravitation is due to the NA^2 terms since gravitation is a small effect which is always attractive. On the other hand, the electrostatic force is assumed proportional to the N^2A^2 terms. For N on the order of 10^{38}, the electrostatic force is 10^{38} times larger than the gravitational force and can be either plus or minus.

It would be natural to assume that the intensity of the wave modes at a particle is primarily due to the interference terms. However, the intensity at a particle is given by

$$I \propto NA^2 \tag{5}$$

since the $2N^2A^2$ terms in equation 4 cancel on the average at an elementary particle, This is understandable because the electrostatic energy is equally plus and minus at a particle. Since only the squared terms remain, the mass energy of elementary particles is then purely gravitational in origin rather than overwhelmingly electrostatic.

3.2   General Force Equation

In order to determine the forces which occur in the wave system, the wave system equation must be solved for small changes in the variable parameters. This assumes that all forces are due to changes in the parameters.

Since the equilibrium solution of the wave system equation is needed, the space dependent eigenvalue equation will be used. This is derived from equation 1 by separation of variables and is

$$\frac{d}{dx}\left(T(x)\frac{dY}{dx}\right) + \sigma(x)(2\pi f)^2 Y = 0 \tag{6}$$

where $(2\pi f)^2$ is the separation constant.

For small spatial variations in the parameters, the perturbative solution of equation 6 is given by

$$
\begin{aligned}
f^2 \;=\; & f_o^2 \left(1 - \frac{2}{L\sigma_o} \int_0^L \left(\sigma(x) - \sigma_o \right) \sin^2\left(kx\right) dx \right. \\
& \left. - \;\frac{2}{kLT_o} \int_o^L \frac{\partial T(x)}{\partial x} \cos\left(kx\right) \sin\left(kx\right) dx \right)
\end{aligned}
\tag{7}
$$

where $f_o = k_o^2/(2\pi)^2 \left(T_o/\sigma_o \right)$ is the unperturbed frequency, σ_o and T_o the average mass density and tension and L is the size of the system. This equation shows that f decreases when $\sigma(x)$ and $\partial T(x)/\partial x$ are larger at the constructive interference peaks.

Equation 8 may be simplified as follows: First, by noting that the last two terms are equal. Second, by setting $\sin^2\left(kx\right)$ and $\sin\left(kx\right)\cos\left(kx\right) = 1/2$ and taking the square root. Then, the perturbed frequency is approximated by

$$
f = f_o \left(1 - \frac{1}{L\sigma_o} \int_0^L \left(\sigma(x) - \sigma_o \right) dx \right).
\tag{8}
$$

Now assume there is only a single particle in the system and the particle or constructive interference peak has a linear width equal to the wavelength, λ. To simplify the nomenclature, set $\sigma = \sigma(x)$. Then, $\sigma = m/\lambda$ and $\sigma_o = m/L$ where m is the mass of the particle. Integrating equation 8,

$$
f = f_o \left(2 - \frac{\lambda\sigma}{L\sigma_o} \right).
\tag{9}
$$

Note: σdx integrates to $\lambda\sigma$ since σ is a constructive interference peak which only exists over one wavelength within the much larger integration distance, L. Without the constructive interference peak, $f = 2f_o$. With the constructive interference peak, $f = f_o$, the stable frequency of the wave system.

Setting $E = hf$, $mc^2 = hf_o$ and $m = L\sigma_o$ in equation 9, we have

$$
\begin{aligned}
E \;=\; & mc^2 \left(2 - \frac{\lambda\sigma}{L\sigma_o} \right) = 2mc^2 - c^2 \lambda\sigma \\
\;=\; & 2mc^2 - \lambda\sigma_e
\end{aligned}
\tag{10}
$$

where σ_e is the energy density (still a function of x). Then the force required to move a mass particle is given by

$$
F = \frac{dE}{dx} = -\lambda\frac{d\sigma_e}{dx}.
\tag{11}
$$

Equation 11 is the "general force equation." The type of force depends upon the nature of the physical process which changes σ_e.

3.3 Derivation of Newton's Law of Gravitation

In a previous paper [14], I derived Newton's law of gravitation from the wave system theory. Because understanding gravitation on a deeper level than Newtonian gravitation or, for that matter, general relativity is essential to the cosmological theories proposed in this paper, I am repeating the derivation in this paper.

To derive Newton's law, assume two protons, labeled m_1 and m_2, are r cm apart. The model for gravitation is as follows: A wave mode originating at m_1 interacts with m_2. Quantitatively, the gravitational force can be calculated from equation 11. The first step is to derive the energy density of a single wave mode at m_2 as a function of r. It is assumed that the initial energy density, σ_e, of a single normal mode is $1/N$ times the energy density at a proton where N is the number of normal modes. Furthermore, the natural assumption in three-dimensional space is that σ_e decreases as $1/r^2$. But differentiating σ_e with respect to r, the force varies as $1/r^3$. This is obviously an incorrect result since the gravitational force experimentally varies as $1/r^2$! But why is this incorrect result obtained?

Assuming the derivation of the general force law is valid, I was forced to reject the isotropic propagation of the normal modes. Instead, I assumed that each wave mode propagates circularly in a plane. The energy density then varies as $1/r$. Although the circular propagation of the normal modes in planes appears physically improbable, I found that the assumption worked perfectly.

Applying this assumption, the energy density of a single normal mode is

$$\sigma_e = \frac{m_1 c^2}{2\pi N r} \text{ erg/cm.} \tag{12}$$

Then, from the General Force Law equation 11, the gravitational force is

$$F = -\lambda \frac{d\sigma_e}{dr} = \lambda \frac{m_1 c^2}{2\pi N r^2} \text{ dynes} \tag{13}$$

where λ is the linear size of an elementary particle, i.e., for a proton $\lambda = 1.3 \times 10^{-13}$ cm.

The dependence of the gravitational force law on the size of the particle is eliminated by the following principle: *The size of a particle is proportional to it's mass.* This follows since the mass density must be the same for all particles; otherwise, energy would be transferred between particles to reach a lower system eigenvalue. We can, therefore, introduce an equilibrium mass density constant for all particles,

$$\sigma_m = \frac{m_p}{\lambda} = 1.28 \times 10^{-11} \text{ g/cm} \tag{14}$$

where the mass of a proton is 1.67×10^{-24} g. The constant, σ_m, explains why the electron is so much smaller than the proton.

To obtain the exact form of Newton's law, multiply equation 13 by m_2/m_2 and set

$$G = \frac{c^2}{2\pi N \sigma_m}. \tag{15}$$

Then, the correct form of Newton's law of gravitation is obtained,

$$F = G\frac{m_1 m_2}{r^2}. \tag{16}$$

This equation has been explicitly derived only for the force between two protons. However, since the forces between pairs of particles are linearly additive, the above equation applies between objects of any mass.

In addition, the number of wave modes can be calculated exactly from equation 15 for G. Solving for N, given $\sigma_m = 1.28 \times 10^{-11}$ g/cm and the known constants,

$$N = \frac{c^2}{2\pi G \sigma_m} = 1.68 \times 10^{38}. \tag{17}$$

N is an important constant in cosmology.

3.4   Circularly Propagating Wave Modes

However, it is still difficult intuitively to make sense of the concept of circular propagation of the modes in an ordinary 3-dimensional space. Fortunately, I was able to prove mathematically that the wave modes propagate circularly by determining that eigenvectors corresponding to circularly propagating wave modes exist in a spherical wave system. The proof depends on the general properties of spherical wave systems and, specifically, on the assumed $1/r$ dependence of the intensity. The wave modes are actually the normal modes of the universe and theoretically completely define the universe. They are a new concept in cosmology and, in fact, their physical existence, to my knowledge, has not previously even been conjectured.

The proof is as follows: Begin with the classical wave equation in spherical coordinates and then consider the separated radial wave equation, $R(r)$, given by

$$\frac{d^2 R(r)}{dr^2} + \frac{2}{r}\frac{dR(r)}{dr} + \left(k^2 - \frac{l(l+1)}{r^2}\right) R(r) = 0 \tag{18}$$

where $k^2 = (2\pi f)^2/c^2$.

The standard method [15] of solving for $R(r)$ is to separate equation 18 into two parts

$$R(r) = r^{-1/2} B(r) \tag{19}$$

where $B(r)$ is Bessel's equation of half-integral order. The solutions of $B(r)$ are non-periodic except when the angular momentum eigenvector $l = 0$. Since periodicity is essential for constructive interference, this is the only solution consistent with the wave system. For this unique solution, the solution is

$$B(r) = \sqrt{\frac{2}{(\pi r)}}\left(\sin\left(r\right) + \cos\left(r\right)\right). \tag{20}$$

However, since $\cos\left(r\right)$ equals 1 at $r = 0$, the factor $\sqrt{(2/(\pi r)}\cos\left(r\right)$ goes to infinity at $r = 0$. Consequently, only the $\sin\left(r\right)$ part of the solution can be

used. However, this is still not the required solution to the problem. Since the intensity I is proportional to $R^2(r)$, I is proportional to $1/r^2$. As previously discussed, this leads to an experimentally incorrect $1/r^3$ law for gravitation based on the general force law.

Nevertheless, the problem can be completely solved by noting that the above formulation of the problem assumes the tension and mass density are uniform for each wave mode. But, this is not true in the wave system since the tension and mass density parameters are assumed proportional to the local intensity of a wave mode. Since the local intensity at r for a circularly propagating wave mode is proportional to $1/r$, we must have $T = T_o/r$ and $\sigma = \sigma_o/r$.

For these parameter variations in the spherical wave equation, the amplitude $B'(r)$ becomes [16]

$$B'(r) = \frac{1}{(T\sigma)^{1/4}} B(r) = \frac{s^{1/2}}{(T_o\sigma_o)^{1/4}} B(r) \tag{21}$$

since $(T\sigma)^{1/4} = r^{-1/2}(T_o\sigma_o)^{1/4}$. Then the radial amplitude function becomes

$$R(r) = r^{-1/2} B'(r) = B(r) \tag{22}$$

and the intensity of $R(r)$ is then proportional to $1/r$, as required. The modes represented by $R(r)$ in equation 22 are very important physically since they are the normal modes of the universe.

What then are the characteristics of this wave model of the universe? First, the normal modes of vibration of the universe are confined to planes orientated in different directions. Each plane is excited as a single mode by a particle and the resulting wave mode propagates circularly in a plane centered on the particle. All the particles in the universe are located on the surfaces of these planes. The three dimensional character of universe is thus made up of a collection of N vibrating planes orientated at different angles and these simulate the isotropic propagation of gravitation.

3.5 Absorption of Gravitation

Consider the case of x-rays incident on a perfect crystal. Experimentally, the x-ray energy density inside the crystal decreases exponentially with distance due to interactions of the x-ray photons with particles within the crystal. By analogy, it is proposed that the intensity of the wave modes are reduced exponentially by absorption and re-radiation by the mass particles. Since the absorbed energy at each interaction of a wave mode is re-radiated in many directions other than the original direction of the wave mode, the intensity of the wave mode along its original direction is reduced. The gravitational force is then reduced in proportion to the decrease in intensity.

Using the theory developed in this paper, the absorption of the wave modes originating from a single proton can be calculated. The energy density of a single mode is given by

$$\sigma_e = \frac{mc^2}{2\pi N s} \exp\left(-s/R\right) = \frac{1.42 \times 10^{-42}}{s} \exp\left(-s/R\right) \text{ erg/cm} \tag{23}$$

where $R = 1.85 \times 10^{28}$ and $N = 1.68 \times 10^{38}$. Note: The variable s will be used from now on for the euclidean distance and r for the normalized distance, s/R.

Equation 23 assumes that the energy density decreases as $1/s$ and is additionally reduced by a factor $\exp{(-s/R)}$ due to absorption by mass particles. Then, the energy, E, absorbed by another proton s distant from the first is

$$E = \lambda \sigma_e = \frac{1.85 \times 10^{-55}}{s} \exp{(-s/R)} \text{ erg} \tag{24}$$

where $\lambda = 1.3 \times 10^{-13}$ cm, the linear size of a proton. $k_o = 1.85 \times 10^{-55}$ is the gravitational absorption constant.

The above absorption theory can be easily applied to a spherical body, such as a star. Consider a spherical distribution of particles with a specific gravity d_{sg} ($d_{sg} = 1$ for water with a density 1.0 g/cm^3). The total energy absorbed from a single proton at the center of the sun is the product of E (equation 24) times the number of protons, n, within a radius s. p is the number of protons per gram, 5.99×10^{23}. Then, the total energy absorption is

$$\begin{aligned} E_{Abs} &= 4\pi p d_{sg} \int_0^r \frac{k_o}{s} s^2 dr = 2\pi p d_{sg} k_o s^2 \\ &= 7.0 \times 10^{-31} d_{sg} s^2. \end{aligned}$$

Since the initial source energy, E_i, is due to a single proton with energy mc^2, the proportion, P, of the gravitational energy shielded is

$$\begin{aligned} P &= \frac{E_{Abs}}{E_i} = \frac{7.0 \times 10^{-31} d_{sg} s^2}{1.50 \times 10^{-3}} \\ &= 4.6 \times 10^{-28} d_{sg} s^2. \end{aligned} \tag{25}$$

For the sun with a radius of 7×10^{10} cm and an average density about 10 times the specific gravity of water, the proportion of the gravitational energy absorbed is about 2.3×10^{-5}. This absorption is negligible and thus confirms current practice of ignoring the possibility of any gravitational absorption for most astronomical bodies. However, for the very largest stars with radii 10^{13} cm (10^8 km), the gravitational absorption approaches 100%.

3.6   Gravity Measurements During a Solar Eclipse

Since the absorption of gravitation is central to the cosmological theories proposed in this paper, the only known observational evidence of gravitational absorption is discussed next. Note that gravitational absorption is not theoretically predicted in either Newtonian gravitation or in general relativity.

From the gravitational theory proposed in this paper, a small absorption of the sun's gravitation by the moon is expected. Recently, the vertical acceleration at the earth's surface during a total solar eclipse in China on March 9, 1997 was accurately measured by Wang [17]. The measurements were corrected for the tidal effects of the sun and moon and for the earth's rotation. These

corrections are accurate to a precision of 1.0×10^{-6} cm/sec^2. Since the results of the gravitational measurements, as described below, were quite different than expected, Wang could offer no explanation of the results but still believed they were a gravitational effect, possibly indicating gravitational shielding by the moon. However, Unnikrishnan [18] has strongly disputed the possibility of shielding of the sun's gravity by the moon based on laboratory gravitational experiments as well as astronomical and planetary observations.

At the time of total eclipse, Wang expected that the measured vertical acceleration towards the earth would increase since the acceleration towards the sun would decrease due to the gravitational absorption of the moon. Contrary to this expectation, the acceleration at the time of total eclipse only shows a small decrease of less than 1.0×10^{-6} cm/sec^2. Instead, two much larger, nearly symmetrical decreases in the measured acceleration occurred before first contact and after fourth contact.

The symmetrical decreases in acceleration are clearly shown in Figure 1 which shows the corrected measurements based on a moving average over three data points. The first, with a maximum decrease of 5.8×10^{-6} cm/sec^2, begins about 120 minutes before totality and ends about 50 minutes before totality. The second, with a maximum decrease of 8.7×10^{-6} cm/sec^2, begins about 50 minutes after totality and ends about 120 minutes after totality. Most important, these are the only statistically significant changes in the gravitational acceleration measured over a period of 1/2 week before and after the eclipse.

It is believed that these observed effects are due to gravitational absorption based on the derivation of Newton's law of gravitation. Any absorption of gravity during an eclipse of the sun by the moon would decrease the acceleration of the earth towards the sun. However, since the earth and the gravity meter are in free fall around the sun, no change in the measured acceleration should occur during a total eclipse.

But, the situation is different for the symmetrical reductions in acceleration. The sun is, of course, eclipsed at other locations before and after the total eclipse at the measurement location. Because the plates of the earth are rigid, it is proposed that the reduction in acceleration of the local plate at these other locations is transmitted to the measurement location and this is what is being measured by the gravity meter. Furthermore, since the strain due to the acceleration is quite small, it is likely that the local plate is freely falling because the stress opposing the acceleration is small.

The reduction in acceleration during an eclipse of the sun can be calculated by the same method used previously to calculate the absorption of gravitation by the mass of the sun. In this calculation, assume a bar of matter, representing a cross section of 1 cm^2 through the moon, has an average specific gravity, σ_{sg}. The ratio of the absorbed gravitational energy to the incident gravitational energy per proton in the sun will give the proportion of the gravitational energy which is absorbed. Then, the reduction in the gravitational acceleration at the earth during a total eclipse will be given by this ratio.

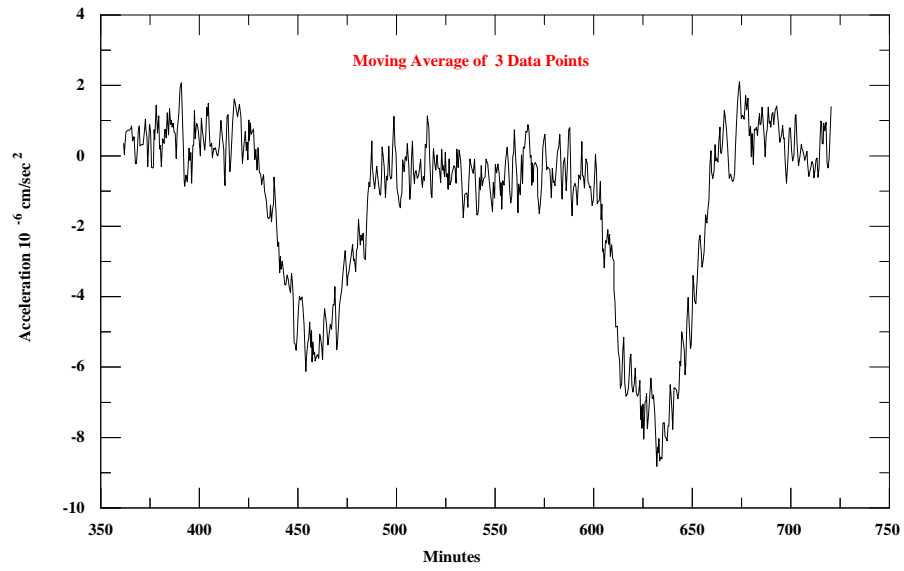Applying this to the solar eclipse, given that the diameter, l_m, of the moon

Figure 1: Measured vertical gravity variations in China during solar eclipse of March 9, 1997. Local time shown in minutes from midnight.

is 3.48×10^8 cm and assuming an average specific gravity of 4, we have

$$E_{Abs} = \frac{p d_{sg} l_m k_o}{s} = \frac{1.48 \times 10^{-22}}{s} \text{ erg/cm}^2. \quad (26)$$

The incident gravitational energy per cm^2 on the bar from one proton in the sun is

$$E_i = \frac{1.5 \times 10^{-3}}{4\pi s^2} = \frac{1.19 \times 10^{-4}}{s^2} \text{ erg/cm}^2. \quad (27)$$

Then, $P = E_{Abs}/E_i = 1.24 \times 10^{-18}$ s. Since the gravitational acceleration of the sun at the earth is 0.59 cm/sec^2 and the distance to the sun is 1.5×10^{13} cm, the reduction in acceleration at the earth during the total eclipse is given by

$$a = -0.59P = -11.0 \times 10^{-6} \text{ cm/sec}^2. \quad (28)$$

Since the sun was at most at an angle of about 23°, the vertical acceleration is $a\sin(23)$ or -4.3×10^{-6} cm/sec^2.

This result is close to the measured symmetrical reductions in acceleration. It is, I believe, a direct observational proof that gravitation is absorbed by matter and justifies using the absorption of gravitation in cosmology. Also note that on the opposite side of the earth from the visible eclipse (the dark side), the symmetrical accelerations should be positive, instead of negative. This provides another opportunity to test the absorption theory of gravitation proposed in this paper.

The above explanation also appears to be confirmed by the comparison of the timing between the optical observations and the events as determined by the measured vertical acceleration data. Table 1 shows the optical times (in universal time) of the eclipseevents [19], the elapsed minutes from 16:00 on March 8, 1997 from optical measurements and from acceleration based measurements.

Comparison of the optical times with the acceleration times shows that the acceleration times are earlier than the optical times. This is expected since theoretically the acceleration times are 500 seconds (8-1/3 minutes) ahead of the optical times. This does not mean that gravitation propagates instantaneously. Instead, the gravitational field, like the electrostatic field, has a velocity-dependent component [20] that cancels the effect of the propagation delay to first order. The difference in the elapsed times between the optical times and the times derived from the acceleration data tends to confirm the theoretical prediction.

4   Cosmological Effects of the Wave System

Assuming the wave system is the basic phenomena of the universe, the dominant effects in the universe must be due to the wave system. These dominant effects are the existence of elementary particles, the energy of mass particles and photons, the mass density of the universe, the Hubble redshift and the size and nature of the universe.

Table 1

Timing of Solar Eclipse Events
March 9, 1997

Eclipse Event	Optical UT	Optical Minutes	Accel Minutes	Diff Minutes
Start Penumbra	23:17:38	438	430	-8
1st Contact	00:03:29	483	471	-12
2nd Contact	01:08:18	548		
Total Eclipse		549.5	540	-9
3rd Contact	01:11:04	551		
4th Contact	02:19:50	620	608	-12
End Penumbra	02:58:23	658	662	4*

*This difference in time is anomalous because there is still more penumbra to the east after the specified "End Penumbra" time. The "End Penumbra" refers to the most extreme southern part of the penumbra, not a later occurring part in the east.

4.1 Mass-Energy of Elementary Particles

To compute the energy absorption by all the protons in the universe, consider a spherical distribution of protons with a number density σ_n. It is assumed that the wave modes originating from a single proton interact with all the protons in the universe. Then, the total energy, E_p, absorbed from a single proton is given by

$$
\begin{aligned}
E_p &= 4\pi\sigma_n \int_0^\infty \frac{k_o}{s} \exp\left(-s/R\right) s^2 ds = 4\pi k_o \sigma_n R^2 \qquad (29) \\
&= 3.0 \times 10^{-55} \, \sigma_n R^2 \text{ erg}
\end{aligned}
$$

where $k_o = 1.85 \times 10^{-55}$ from equation 24 and σ_n is the number density of particles.

This result identifies the source of the mass energy of elementary particles with the mutual interactions between all the particles in the universe. This explanation is consistent with an equilibrium state of the universe because the input energy to a particle equals the output energy of a particle.

4.2 Predicted Mass Density of the Universe

Given the energy of a proton, σ_n can be calculated if R is known. For $R = c/H$ (section 5) and $H = 50$ km/sec/Mpc, $R = 1.85 \times 10^{28}$ cm. R is the mean absorption distance in the universe. Then, σ_n is given by

$$
\sigma_n = \frac{E_p}{4\pi k_o R^2} = 1.8 \times 10^{-6} \text{ particles/cm}^3. \qquad (30)
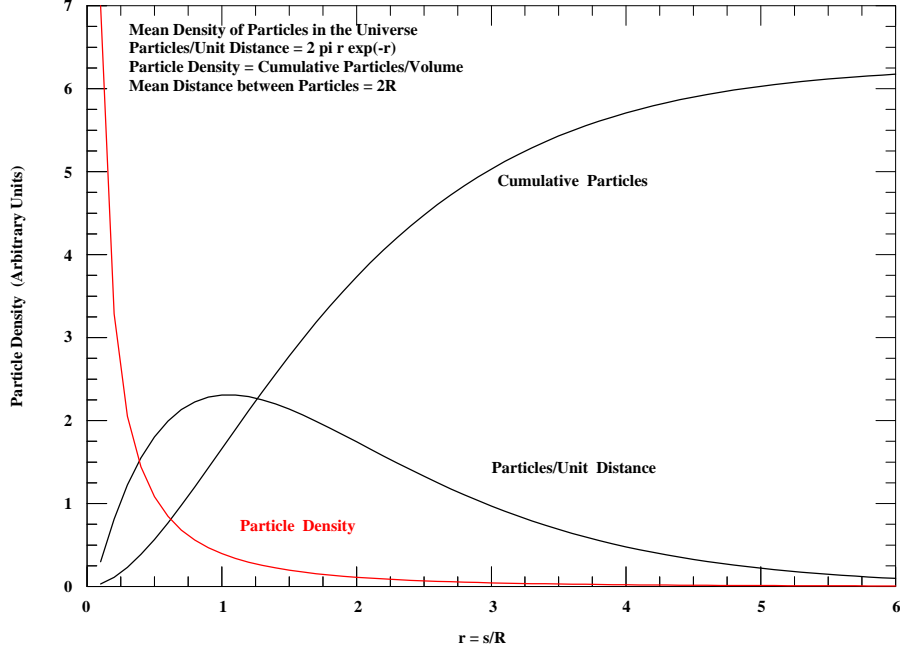$$

19

Figure 2: Density of particles assuming circularly propagating planes model of the universe. The mean particle density is given by the particle density at the mean distance between particles, $s = 2R$.

Then, the average mass density of the universe, σ_d, with $m_p = 1.67 \times 10^{-24}$ g is given by

$$\sigma_d = m_p \sigma_n = 3.0 \times 10^{-30} \text{ g/cm}^3. \tag{31}$$

This mass density is a factor about ten times greater than is observed. Previous predictions were even larger in the expanding universe models and, therefore, prompted the idea of "missing mass." With this prediction, the amount of missing mass is reduced but there is still a very appreciable difference between theory and observation.

Because of the above inconsistency between theory and observation, it is believed that the above theory is incorrect. Thus, an alternate theory is proposed.

The structure of the universe is really determined by the circularly propagating planes which assumes the particles exist only on the surface of the planes. This is a very different concept from the concept of a random location of particles in a three dimensional space. The mass density given by equation 31 was based on this concept and, therefore, the result is clearly suspect.

Using the concept of circularly propagating planes, the energy of a particle

is instead given by

$$E_p = 2\pi N \sigma_s \int_0^\infty \frac{k}{s} \exp\left(-s/R\right)s \ ds = 2\pi N k_o \sigma_s R. \tag{32}$$

From this equation, the surface density of particles, σ_s, is

$$\sigma_s = \frac{E_p}{2\pi N k_o R} = 4.0 \times 10^{-16} \text{ particles/cm}^2. \tag{33}$$

It is difficult to relate this to the previous particle density result of 3.0×10^{-30} g/cm^3 because one measure is in cm^3 and the other in cm^2.

To determine the mean number density (and the mean mass density), first calculate the cumulative number of protons, n_p, versus s. n_p is given by

$$n = 2\pi N \sigma_s \int_0^s \exp\left(-s/R\right)s \ ds = 2\pi N \sigma_s R^2 \left[1 - (s/R + 1)\exp\left(-s/R\right)\right]. \tag{34}$$

Then, the proton number density can be computed by dividing n by the Euclidean volume at s. This is shown graphically in Figure 2 (for N and $\sigma_s = 1$). For small s, the proton number density is large but falls rapidly as s increases. The question is "What volume should be used as a measure of the proton number density?" Since the mean distance between protons is $s = 2R$, the volume at this mean distance seems appropriate as a measure of the mean proton number density. Setting s equal to $2R$, the mean number density of protons is

$$\sigma_n = \frac{n}{4\pi/3(2R)^3} = \frac{3N\sigma_s}{16R}\left(1 - 3\exp\left(-2\right)\right) = 3.9 \times 10^{-7} \text{ particles/cm}^3. \tag{35}$$

From this result, the mean mass density of the universe is

$$\sigma_d = 1.67 \times 10^{-24}\sigma_n = 6.6 \times 10^{-31} \text{ g/cm}^3. \tag{36}$$

This mean mass density is close to the observed mean mass density of matter in the local universe.

4.3   Size and Nature of the Universe

Given a static and equilibrium (non-evolving) universe, the determination of the size and age of the universe may be logically deduced from the wave system model. A starting point is the observation that the physical constants [9] are exactly the same in very distant galaxies. Then, assuming the physical constants are a function of the frequency and number of wave modes, particles in distant galaxies must interact with the same effective number of distant particles as local particles. However, these distant particles interact with a different set of particles than the local particles do since all interactions decrease exponentially with distance due to absorption of the wave modes. Since distant galaxies interact with even more distant particles than local galaxies, I conclude that the universe must be very much larger than R, the absorption (or interactive)

radius of the universe, or even infinite. Finally, an infinite universe implies an infinitely old universe since interactions at the velocity of light will take an infinite time to traverse an infinite universe.

If the static universe is infinite (or very much larger than R), some consequences are:

1. The gravitational potential must be finite and the same at all points (except near large masses) since each mass particle interacts gravitationally with the same finite effective number of particles. The universe on a large scale then must be flat (Euclidean).

2. In an infinitely old universe, the universe must be non-evolving on a large scale. Therefore, the properties of clusters and galaxies must on the average be independent of time and independent of their distance from us. This is another argument for the PCP and an equilibrium universe.

3. A corollary is that processes must exist which maintain the universe in an equilibrium state. The determination of these processes should be a goal of future astrophysical research.

One process proposed by Moore [21] could maintain a non-Maxwell-Boltzman distribution of the particles in an infinite universe and prevent "the heat death of the universe". The process is based on the principle that the momentum of a gas filling an infinite volume must be zero with respect to all inertial frames. As a result of this principle, the infinite system can not reach a Maxwell-Boltzman equilibrium. Nevertheless, localities do tend towards a localized equilibrium but this equilibrium is upset at random times by collisions with other localities. If this process does exist, observers would always perceive a non-equilibrium state when they look out in space with telescopes. Then, the "stable state" of the universe must be a dynamic state involving constant change.

5   Hubble Redshift Process

I assume the Hubble redshift is due to a physical process instead of the expansion of the universe. However, the derivation of a physical process for the Hubble redshift is a difficult problem. To my knowledge, all previous attempts to derive a physical process have not been viable. It is also clear that because the redshift is a global process, the redshift is telling us something new about the basic workings of the universe. After all, a photon's energy is reduced by about 2/3 if it originates at $z = 1$. This reduction in energy, if applied to an ultraviolet photon, amounts to a large amount of energy. Where does the energy go? The difficulty of the problem is due to the few clues to the physical nature of the Hubble redshift.

Only one of the many theorists who attempted to derive a physical process for the Hubble redshift will be specifically mentioned. Furth [22] hypothesized that gravitational effects are responsible for the redshift and attempted to link the Hubble redshift to similar redshifts occurring in the spectral lines near the

sun's limb. Specifically, he proposed that photons forced to move along a curved path in a gravitational field would loose energy. From this argument, he could show that a redshift approximately proportional to the observed redshift would occur. However, the complexity of the hypothesis and the uncertainties of the physical explanation made the physical process unlikely. Nothing ever came of his hypothesis.

Early on, I concluded that new physics was required because no solution to the redshift problem had been found, despite the many theorists who worked on the problem. The Hubble redshift appears to be a basic problem on a par with other unsolved basic problems of physics. In the last section, new physics was developed involving the concept of an underlying wave system. This lead to the concept that the mass energy of particles is due to interactions between particles.

The energy exchange, δE, between two particles is proportional to

$$\delta E \propto \frac{\exp\left(-s/R\right)}{s} \tag{37}$$

where R is the mean absorption distance in the universe. The energy of a mass particle or a photon is, therefore, the sum of these energy exchanges.

Given the above model for the energy of a particle, a local particle moved to another location will be further from some particles and closer to others. As a result, a net reduction in the energy of the local particle will be shown to occur. It is this reduction in energy which produces the Hubble redshift of photons.

This model has been simulated on a computer by assuming a particle moves a small distance s (to the right) along the x-axis. The interaction of distant particles with the local particle is represented by equation 37. The simulation shows that the energy of a photon or a mass particle is reduced by

$$\delta E = -\frac{s}{R}E \tag{38}$$

when it moves a distance s in any direction. E is the initial energy of a mass particle or a photon. The computer program used for the simulation is shown in Appendix A with a printout of results from one simulation.

However, the simulation is complicated because it takes place in an infinite universe where the "cut-off" of distant particles is soft due to the the exponential term in equation 37. Therefore, I have devised a simplified model to understand why the energy reduction in the simulation occurs.

In the simplified model, the universe is represented by a plane circle with a local particle at the center. The radius of the circle is large enough ($s > R$) so that particles at a greater distance (outside the circle) interact very little with the local particle. The model, therefore, includes essentially all the particles in the universe which significantly interact with the local particle. Furthermore, these interacting particles can be considered fixed in position as the local particle moves. This model is shown in Figure 3A.

For the simulation, the universe is assumed very large and divided into three regions, A, B and C. This division is shown schematically in Figure 3B. The
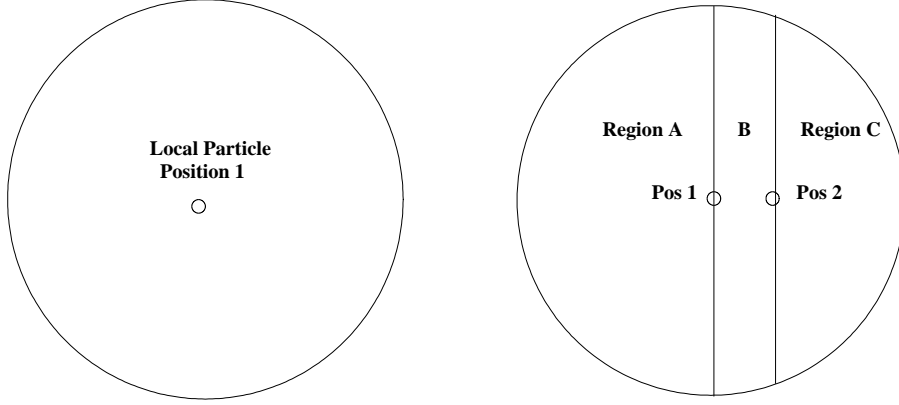
Figure 3: Simplified model of the universe. In the left-hand circle, a local particle in position 1 interacts with all the particles in the universe. In the right-hand circle, the local particle moves to position 2 where it interacts with the same particles. The decrease in the interaction energy is responsible for the Hubble red shift.

number of effective particles interacting with the local particle in the simplified model is proportional to the areas of the separate regions in the circle.

Assume the local particle is initially located at position 1 and, subsequently, moves a distance, s along the x-axis to position 2. The reduction in energy when the particle moves from position 1 to position 2 is determined separately for each region. Wave modes from two particles located in each region to the local particle will be modeled. To simplify the bookkeeping, the contribution of energy from each region to the particle in positions 1 and 2 will be shown in Tables 1A, 1B and 1C.

Mass particles are assumed to result from the constructive interference of wave modes moving in opposite directions to produce a standing wave. In contrast, a photon is considered a result of wave modes propagating in the same direction as the photon. Alternatively, the photon can also be considered a standing wave effect. In any case, both assumptions will be shown to give the same result for the photon.

First, consider wave modes coming from particles in the left hand region of the circle, labeled A, and interacting with the particle in position 1. The energy absorbed is proportional to the area of A. This area is $1/2$ the full area of the universe and contributes energy $E/2$. This is shown in Table 2A as "$E/2$" for region A and position 1.

Wave modes coming from regions B and C also interact with the particle in position 1. The total energy received from both regions is $E/2$. However, this energy will be separately accounted for in each region. $E/2(s/R)$ comes from region B and $E/2(1 - s/R)$ comes from region C. These are shown in Table 2A for position 1 as $E/2(s/R)$ for region B and $E/2(1 - s/R)$ for region C.

Table 2A
Decrease in Energy of a Mass Particle
Moved from Position 1 to Position 2

Particle Position	Region A	Region B	Region C
$P1$	$E/2$	$E/2(s/R)$	$E/2(1-s/R)$
$P2$	$E/2(1-2s/R)$	$E/2(s/R)$	$E/2$
P2 less P1	$-E(s/R)$	0	$E/2(s/R)$
Net Decrease	$-E/2(s/R)$		

When the particle is in position 2, the particles in region A are at a greater distance from the local particle. In the simulation, the energy received from each particle in A is given by

$$\delta E \propto \frac{\exp{(-s/R)}}{s} \qquad (39)$$

where $s = \sqrt{(x+s)^2 + y^2 + z^2}$ for $x => s$. The energy absorbed from region A is $E/2(1-2s/R)$. The first s/R is due to the greater distance of the particles. The second s/R is due to the smaller number of particles since region B is not included in the sum. Finally the energy received from B is $E/2(s/R)$.

The particles in region C are closer for the particle in position 2. Again, the energy received from the particles in region C is given by

$$\delta E \propto \frac{\exp{(-s/R)}}{s} \qquad (40)$$

where $s = \sqrt{(x-s)^2 + y^2 + z^2}$ for $x => s$. The energy absorbed from region C is $E/2$. This is same as the energy absorbed from region A but this result is due to two compensating effects. The closer particles increase the energy by $E/2(s/R)$ but the fewer particles in region C reduce the energy by the same amount.

In Table 2A, if the energy associated with the particle in position 2 is subtracted from position 1, the net decrease in energy is $-E(s/R) + E/2(s/R) = -E(s/(2R))$. However, this result must be revised as follows: The input energy to position 2 from region C is nominally $E/2$. But, as in gravitation, the energy absorbed is proportional to the energy of the absorbing particle. The energy of the particle has been reduced already by $E/2(1-s/R)$, the sum of the energies from regions A and B for position 2, Consequently, the input energy to position 2 from region C is reduced to $E/2(1-s/R)$. This is shown in Table 2B. Then, the net decrease in energy $(P2 - P1)$ is $-E(s/R)$.

For the photon, Table 2C shows the energy changes. As before, the energy is reduced by $E(2s/R)$ but at the same time there is an increase in energy from region B. The net decrease is, therefore, $E(s/R)$. But note that this applies to the total energy of a photon propagating to the right. Therefore, the net reduction in the energy, E, of a photon is the same as for a mass particle.

<div align="center">

Table 2B
Revised Decrease in Energy of a Mass Particle
Moved from Position 1 to Position 2

</div>

Particle Position	Region A	Region B	Region C
$P1$	$E/2$	$E/2(s/R)$	$E/2(1-s/R)$
$P2$	$E/2(1-2s/R)$	$E/2(s/R)$	$E/2(1-s/R)$
P2 less P1	$-E(s/R)$	0	0

<div align="center">

Table 2C
Decrease in Energy of a Photon
Moved from Position 1 to Position 2

</div>

Particle Position	Region A	Region B	Region C
$P1$	E	0	
$P2$	$E(1-2s/R)$	$E(s/R)$	
P2 less P1	$-E(2s/R)$	$E(s/R)$	
Net Decrease	$-E(s/R)$		

This reduction in energy produces redshifts photons or acts to de-accelerate a mass particle, assuming the mass particle has kinetic energy. Of course, to move an intially stationary particle, the "Hubble" force (in addition to the ordinary inertial force) is required to move a mass particle.

5.1   Photon Redshift

Let the particle moving to the right be a photon. The reduction in the energy is given by Table 2C. Consequently, the energy of a photon decreases as it moves a small distance ds. This energy decrease is given by

$$dE = -\frac{ds}{R}E \tag{41}$$

where E is the original energy of the particle and $R = c/H$ is the mean absorption or interaction distance of the wave modes. Integrating the above equation, $\ln(E/E_o) = -s/R$ or $E = E_o \exp(-r)$ where the normalized distance $r = s/R$. Then, from the relation, $f = E/h$, the redshifted frequency, f, is given by

$$f = f_0 \exp(-r). \tag{42}$$

For small values of the redshift, r is equal to z. For large values of the redshift, $r = ln(1+z)$.

This process is proposed as the cause of the observed Hubble redshift of photons. Since the redshift is a pure gravitational effect, the energy of the photon is reduced without any blurring of distant galaxies.

5.2 Mass Particle Redshift

The redshift has an equal effect on the mass particle. Thus, the decrease in the energy of the particle (see Table 2B) as it moves a small distance ds is given by

$$dE = -\frac{ds}{R}E. \tag{43}$$

This mass particle "redshift" possibly explains a part of the observed, very small, anomalous acceleration toward the sun of the Pioneer 10 and 11 spacecraft [23]. An expression for the acceleration can be derived from equation 43 by setting $dE/ds = ma$ and using the relations $E = mc^2$ and $R = c/H$. Then, the acceleration due to the redshift of mass particles is

$$a = -cH. \tag{44}$$

This acceleration is directed towards the sun.

For $H = 59$ (5) km/sec/Mpc [24], the predicted acceleration is 5.6 (0.7) $\times$ 10^{-8} cm/sec^2. This compares with the recent result on the anomalous acceleration [25] of 8.74 (1.25) $\times 10^{-8}$ cm/sec^2 directed towards the sun for Pioneer 10 and 11. The difference between the predicted and observed accelerations could well be due to a small non-isotropic power radiation of the Pioner equipment directed away from the sun as discussed by Scheffer [26].

The mass particle redshift also tends to prevent very large mass accumulations in the universe since it limits the distance a particle can move, given an initial kinetic energy.

6 Time-Dilation Process for Supernovae

Observations of supernovae by Goldhaber [27] show that the period of the light curve of a supernovae is time-dilated proportional to $(1 + z)$. In the expanding universe model, this effect is explained as follows: Because photons produced at a later time have to travel a longer distance to the observer than photons produced at an earlier time, the observed photons are spread over a longer time interval. Since this process does not occur in a static universe, it is generally considered that the existence of time-dilation proves that the universe is expanding.

Normally, if the universe is static, there should be no time-dilation. This is true for elliptical galaxies since their luminosity is completely accounted for without consideration of time-dilation. However, the physical situation is different for supernovae. The luminosity of a supernovae varies significantly over the period it is visible. Therefore, it is proposed that the varying luminosity in conjunction with the redshift produces a time-dilation. This increases the period of the supernovae in the observer's rest frame and reduces the luminosity of the supernovae.

Quite by chance, I came across a letter to the editor by Noerdlinger [28] that discusses the time-dilation of quasars. Noerdlinger was concerned with

determining the diameters of quasars from observed fluctuations in luminosity. The following quote from the letter describes his theoretical reasoning:

> Think of the fluctuation of any one spectral line as amplitude modulation of a carrier. Since waveforms are preserved by the redshift, the maxima in amplitude must have the same relation to the oscillations of the carrier before and after redshifting, and so must become similarly spread out in time. This argument is independent of the cause of the redshift. Suppose, now, that an observer near the quasi-stellar object sees it fluctuate with period T_o, and so would say that it's diameter could not exceed $d = cT_o$. The terrestrial observer sees a period redshifted to the value $T = T_o(1 + z)$. Thus $T_o = T/(1 + z)$ and the correct value of d is $d = cT/(1 + z)$.

This physical theory of time-dilation for quasars is directly applicable to supernovae. Thus, the large variation in luminosity of a supernovae increases the period, T_o, of the light curve of supernovae by the factor $(1 + z)$.

I have an equivalent physical argument for the time-dilation. Since all frequencies are reduced by the Hubble redshift, the light curve modulation frequency is also reduced. This reduction in frequency corresponds to an increase in the original period, T_o, of the light curve by $(1 + z)$. Thus, the whole light curve of a supernova is time-dilated as observed in the observer's rest frame. Since this reduces the number of photons received per second by the observer, the light intensity is reduced. It follows that the apparent magnitude is increased by $2.5 \log(1 + z)$.

Furthermore, since the above process is independent of the cause of the redshift, it must also occur for supernovae in the expanding universe models. However, this creates a fatal problem for expanding universe models. The expanding universe already incorporates a time-dilation effect which affects any luminous object equally. Thus, in the expanding universe model, the time-dilation due to the variation of the supernovae light curve is a second time-dilation effect. Since only a single time-dilation effect was observed by Goldhaber, the expanding universe model must be considered logically falsified. Of course, no such logical problem occurs in the static universe model. Only one time-dilation effect occurs for supernovae in the static universe model and this agrees with the observations.

7 Cosmic Microwave Background Process

To derive the cosmic microwave background (CMB) process, the key assumption proposed by Hoyle [29] is that iron whiskers occur throughout space with a mass density, σ, and have the large absorption coefficient, $k = 3 \times 10^7$, in the microwave region. Outside the microwave region, the iron whiskers have the much smaller absorption coefficient, $k = 10^4$. Consequently, the iron whiskers do not affect observations by optical or radio telescopes. If this assumption is

correct, it is only necessary to show that the source of the energy in the CMB is redshifted visible and ultraviolet starlight.

In this connection, Burbidge [30] has shown that if the mass density is about 3×10^{-31} g/cm^3 and the He/H ratio by mass is 0.244, then the energy released is 4.4×10^{-13} erg/cm^3. If this energy is thermalized, the CMB black body temperature is $T = 2.76^o$ K which is close to the observed 2.73^o K.

Given that the static universe is infinite in size, it is shown below that visible and ultraviolet starlight can be redshifted to microwave frequencies with an increase in intensity. Using the normalized distance $r = s/R$,

$$I_T = 4\pi \int_0^\infty \frac{I_o}{4\pi r^2} \exp\left(-r\right) r^2 dr = \int_0^\infty I_o \exp\left(-r\right) \, dr = I_o. \qquad (45)$$

The integration above is over an infinite universe where I_o is the average intensity of starlight emitted from one cubic centimeter of space. The exponential factor here is due to the Hubble redshift. Remarkably, this sum equals the initial intensity (ignoring the small absorption in the visible region), i.e., $I_T = I_o$ except that the redshift reduces the average frequency by one-half.

Moreover, since the sum, I_T, occurs at all points (particles) in an infinite universe, I_T can be redshifted again to obtain the same intensity which is further reduced in frequency by one-half. After about 10 such redshifts, the frequency of I_T is in the microwave region where the redshifted starlight can be absorbed by the iron whiskers. Note: The absorption by the iron whiskers in the microwave region limits further integrations. At the same time, the redshifted light intensity is increased by a factor of 5 to 10 by the multiple redshifts. This process admittedly appears strange but, nevertheless, I believe it does occur.

Assuming the CMB radiation field is in equilibrium, the intensity loss from the CMB field due to the Hubble redshift must equal the input intensity from the redshifted visible light. Let the average normalized distance traveled by a CMB microwave photon between emission and absorption equal r. Then, the decrease in the CMB intensity is given by

$$\Delta B = B(1 - \exp\left(-r\right)) \qquad (46)$$

where B is the CMB radiation intensity. Given that $\Delta B/B \approx 1/25$, $r = 0.04$. For $B = 1.2 \times 10^{-2}$ erg/cm^2/sec, this requires that $\Delta B = 4.8 \times 10^{-4}$ erg/cm^2/sec. This intensity, ΔB, is the same order of magnitude as the total redshifted starlight. Totani [31] cites current measurements of the extragalactic background light in the near infrared in the range 20 to 30 nW/m^2/sr. This is equivalent to 1.0×10^{-4} to 1.5×10^{-4} erg/cm^2/sec. This intensity is slightly smaller than the ΔB required to maintain the equilibrium of the CMB. Still, it appears the CMB is in an equilibrium state consistent with the intensity of light emitted by the stars and the reduction in the CMB intensity due to the Hubble redshift.

For a single absorption and emission in the distance r, the required mass density of the iron whiskers is given by $\sigma = 1/(tkc)$ where $t = rR/c$. Thus, for $r = 0.04$, $R = 1.85 \times 10^{28}$ cm and $k = 3 \times 10^7$, $\sigma \approx 10^{-34}$ g/cm^3. While

this mass density of iron whiskers is large, it is possible if the iron whiskers accumulate in extragalactic space over very long periods of time (say 50×10^9 years) between recycling. Since Hoyle has estimated that the production of iron by supernovae explosions over 10×10^9 years results in an iron density of about 10^{-35} g/cm^3, an iron density of 10^{-34} g/cm^3 seems reasonable.

The number of absorptions and emissions for $r = 0.04$ is on the order of 25, more than sufficient to thermalize and smooth the CMB field. Furthermore, the CMB intensity should be uniform throughout the universe since the iron whiskers are evenly distributed in extragalactic space due to radiation pressure.

8   Observational Tests

The observational tests in this paper include surface brightness, apparent magnitude, angular size and galaxy counts. These are the same tests suggested by Sandage [32].

First-rank elliptical galaxies and supernovae are the objects most useful in determining the space-time metric of the universe. Both have absolute magnitudes that are nearly the same and thus they are referred to as standard candles. First-rank elliptical galaxies are more luminous than supernovae and can measure the metric at larger distances. On the other hand, supernovae are better standard candles.

Elliptical galaxies of different luminosities and sizes can also be used to measure the metric by making use of relations between the luminosity, the metric size and the velocity dispersion of the galaxies. These relations can be determined at low z and then applied to elliptical galaxies at greater z. These relations are collectively referred to as the "Fundamental Plane." The advantage to using cluster elliptical galaxies is that they are many times more numerous than first-rank elliptical galaxies and will have different evolutionary histories.

The data for the tests was obtained from refereed papers published within the last 10 years (with several exceptions). The data are quantitative, and most important, accurate enough to distinguish between different models of the universe.

Of course, the observational data must first be corrected by the K-correction. The K-correction compensates for the changes in the observed spectrum of a galaxy as a function of the redshift, z. Assuming the filter bandwidth is fixed, the K-correction also includes a correction factor for the observed decrease in luminosity due to the $(1 + z)$ wavelength stretching in the observer's rest frame.

For the static universe model, the observed slope, its standard deviation and the standard deviation for the individual galaxy observations are shown on each graph. Descriptions of the mathematical models and the methods used for analysis of the observational data using the static universe model are given in the following sections.

For various reasons, there are usually a few outliers in a set of data. Outliers are defined as values which are more than 2.5 standard deviations from the theoretically expected value. Since these outliers have a disproportionate effect

on the data average, I discard these outliers. With good data, the number of outliers generally do not exceed 5% of the data. When this is the case, I find that the data set is significantly improved without any compromise in the integrity of the data.

9   Surface Brightness

The surface brightness test will be discussed first. It is the only observational test which discriminates between any expanding universe model and the static universe model. Two surface brightness tests were made, each based on a different data set.

The first data set includes only first-rank elliptical galaxies. This data set was compiled from the observational studies of different observers. Below $z = 0.1$, the data is from ground based observations. Above $z = 0.1$, the data is from HST observations. All of the data is based on similar data reduction procedures. K-corrections were generally made by the observers and were incorporated in their listed data.

The second data set consisting of cluster elliptical galaxies was compiled by Kochanek [33] also from observational studies of different observers. However, to insure uniformity in the measurement of the galaxy parameters, Kochanek re-measured the parameters of each galaxy in the different studies. Kolchanek did not estimate the K-corrections or the galactic absorptions for the individual clusters. I determined the K-corrections from Fukugita [35] and calculated the galactic absorptions from the foreground galactic extinctions $E(B - V)$ which were provided by Kochanek and an $R = 3.1$ extinction curve.

In contrast to the first data set, the set from Kochanek consists of elliptical galaxies of widely different luminosities and physical sizes. Consequently, before the surface brightness test can be applied, the galaxies must be normalized to a standard elliptical galaxy using the fundamental plane method. I arbitrarily chose a standard elliptical galaxy with an effective radius of 10 Kpc and a velocity dispersion of 225 Km/sec.

Both sets of data are also used for Euclidean apparent magnitude tests. In addition, the first-rank elliptical galaxy set is used for the angular size test of the metric. The two sets of data are listed in Tables 3A, 3B, 4A and 4B.

Figure 5 shows frequency distributions of the parameters of the first set of data. The parameters of the first-rank elliptical galaxies are computed based on the static universe model cosmology. The frequency distributions show nothing unusual about the test sample of first-rank elliptical galaxies.

Figure 7 shows a frequency distribution of the parameters of the second set of data (less 3 outliers). However, for this set, the parameters of the cluster elliptical galaxies are derived based on the standard elliptical galaxy. Again, the frequency distributions show nothing unusual about this test sample.

The surface brightness is given by

$$SB = m_e + 2.5 \log \left(\pi \theta^2 \right) \tag{47}$$

31

where SB (in mag/θ^2) is the surface brightness, θ is the effective (half-light) angular radius and m_e is the apparent magnitude within the effective angular radius.

In the flat, static universe model, the observed surface brightness varies with redshift as

$$SB(z) = 2.5 \log (1 + z) + SB(0). \tag{48}$$

Thus, when the surface brightness versus $2.5 \log (1 + z)$ is plotted, the plot theoretically is linear with slope 1.

In the expanding universe models, the observed surface brightness varies theoretically as

$$SB(z) = 4 \left[2.5 \log (1 + z) \right] + SB(0) \tag{49}$$

and, thus, is linear with a slope of 4. It is important to note that this slope applies to all of the expanding universe models. Thus, the slope of the surface brightness versus $2.5 \log(1 + z)$ can clearly determine whether the universe is static or expanding.

9.1   First-Rank Elliptical Galaxies — Many Observers

For first-rank elliptical galaxies, the surface brightness test is straightforward because it is based only on observational data. Since first-rank elliptical galaxies were not generally identified in the observations, it was assumed the brightest elliptical galaxy in a cluster was, in fact, a first-rank elliptical galaxy. To further assure that only first-rank elliptical galaxies were selected, elliptical galaxies were required to have, in the static universe model cosmology, an absolute magnitude in the Johnson B band brighter than -22.2 magnitudes and an effective physical radius between 25 and 75 Kpc. The restriction on size was to avoid extreme examples of first-rank elliptical galaxies.

The Johnson B band was selected as the common band for the surface brightness data since most of the galaxies were observed in the B band. There were some problems encountered in using the data. In many cases, the expected surface brightness dimming in the expanding universe model of $10 \log (1 + z)$ was subtracted from the observational data and, therefore, had to be added back to obtain the correct observational data. In other cases, the surface brightness was calculated from the listed absolute magnitude and the effective angular radius. And, of course, data observed in other bands was converted to the Johnson B-band using the conversion tables of Fukugita [35]. After these conversions were made, the observational data was directly plotted against $2.5 \log(1 + z)$.

Figure 4 shows that the surface brightness observations fit the static universe model very well. The least squares regression for the surface brightness is given by

$$SB = 1.08 \left[2.5 \log (1 + z) \right] + 23.69. \tag{50}$$

The ordinate in this equation is $2.5 \log (1 + z)$. The observed slope is 1.08 which, with a standard deviation of 0.21 magnitudes, quite clearly confirms the static universe model and excludes the expanding universe models.

32

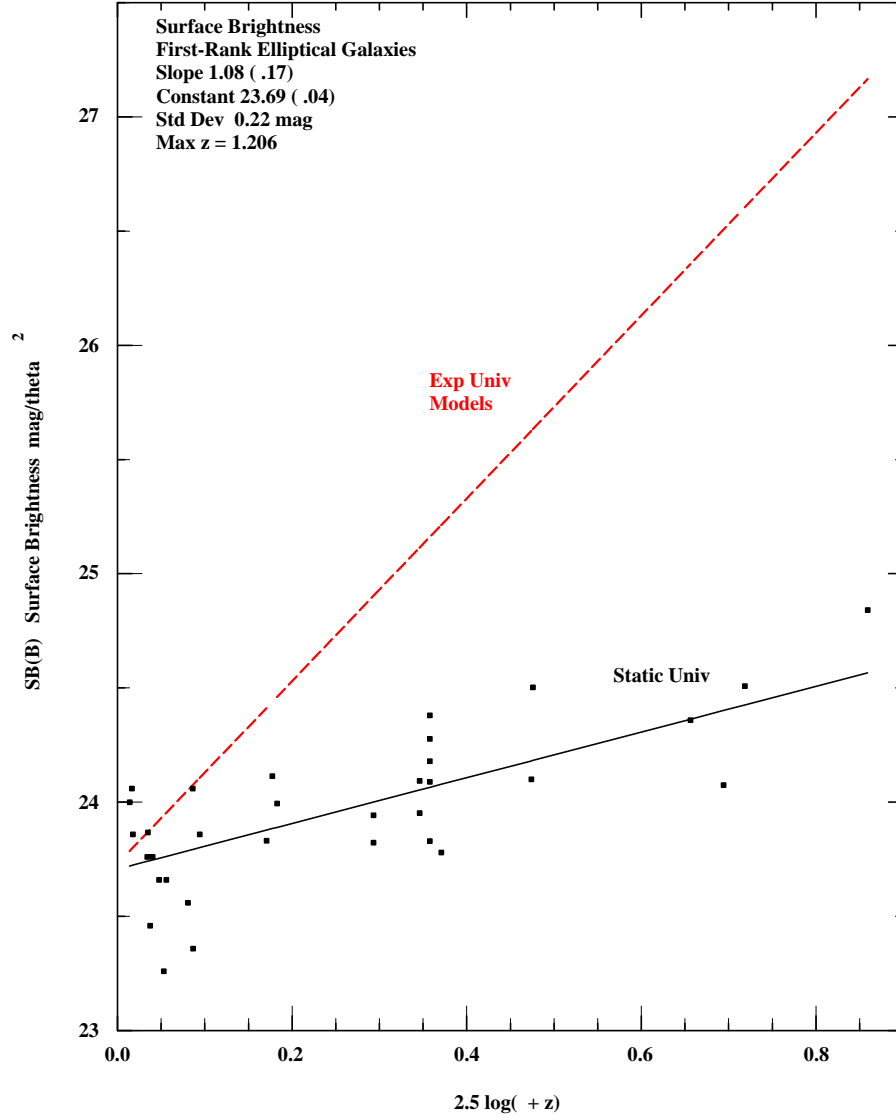Figure 4: Surface brightness of first-rank elliptical galaxies. The black squares represent the surface brightness observations and the black line is the static universe regression line with a theoretical slope of 1. The dashed red line has a theoretical slope of 4 in expanding universe models.
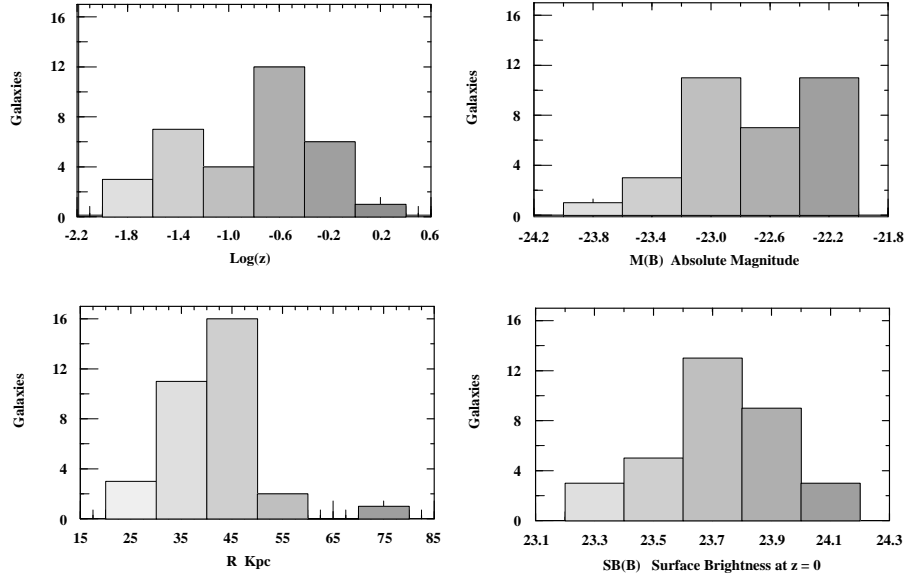
Figure 5: Distribution of static universe parameters of test sample of first-rank elliptical galaxies.

Table 3A
Analysis of First-Rank Elliptical Galaxies
Static Universe Model Parameters

Galaxy	Observer & Ref	z Data	r	SB Data	Data Band	Corr to B	SB(B) Corr
Hydral N3311	Jorgensen [36]	0.0129	0.0128	23.17	Gunn g	0.83	24.00
AWM3 N5629	Sandage [37]	0.0152	0.0151	23.1	V	0.96	24.06
A262 N708	Sandage [37]	0.0164	0.0163	22.9	V	0.96	23.86
A496	Sandage [37]	0.0316	0.0311	22.8	V	0.96	23.76
A539 d47	Jorgensen [36]	0.0324	0.0318	23.04	Gunn g	0.83	23.87
A2052	Sandage [37]	0.0348	0.0342	22.5	V	0.96	23.46
A1139 U6057	Sandage [37]	0.0376	0.0369	22.8	V	0.96	23.76
A119	Sandage [37]	0.0446	0.0436	22.7	V	0.96	23.66
A85	Sandage [37]	0.0499	0.0487	22.3	V	0.96	23.26
A978	Sandage [37]	0.0527	0.0514	22.7	V	0.96	23.66
A2255	Sandage [37]	0.0769	0.0741	22.6	V	0.96	23.56
A2420	Sandage [37]	0.0823	0.0791	23.1	V	0.96	24.06
A1126	Sandage [37]	0.0828	0.0796	22.4	V	0.96	23.36
A2440	Sandage [37]	0.0904	0.0865	22.9	V	0.96	23.86
A2218	Barger [38]	0.170	0.157	23.83	B	0.00	23.83
A2218-L244	Jorgensen [39]	0.177	0.163	23.16	V	0.96	24.12
A665-1150	Jorgensen [39]	0.183	0.168	23.04	V	0.96	24.00
AC103(1)	Barger [38]	0.310	0.270	23.94	B	0.00	23.94
AC103(2)	Barger [38]	0.310	0.270	23.82	B	0.00	23.82
MS1512+36	Bender [40]	0.375	0.318	23.95	B	0.00	23.95
A370 20	Barger [38]	0.375	0.318	24.09	B	0.00	24.09
CL0024 186	van Dokkum [41]	0.390	0.329	23.45	Gunn g	0.83	24.28
CL1447(1)	Barger [38]	0.390	0.329	24.18	B	0.00	24.18
CL1447(2)	Barger [38]	0.390	0.329	24.38	B	0.00	24.38
CL1447(3)	Jorgensen [39]	0.390	0.329	24.09	B	0.00	24.09
CL1447(4)	Barger [38]	0.390	0.329	23.83	B	0.00	23.83
Abell 851	Dickenson [42]	0.407	0.341	23.78	B	0.00	23.78
CL0016	Schade [43]	0.547	0.436	24.10	B	0.00	24.10
CL1601(2)	Barger [38]	0.550	0.438	24.50	B	0.00	24.50
MS1054 1484	van Dokkum [44]	0.830	0.604	23.77	F814W	0.59	24.36
CL1603-431	Dickenson [42]	0.895	0.639	24.08	B	0.00	24.08
03.1077	Schade [45]	0.938	0.662	24.51	B	0.00	24.51
3C324	Schade [43]	1.206	0.791	24.84	B	0.00	24.84
53W002*	Pascarelle [46]	2.390	1.221				

* Angular radius only, surface brightness data unreliable.

Table 3B
Analysis of First-Rank Elliptical Galaxies
Static Universe Model Parameters

Galaxy	Disp Data	Disp Stat	θ_e Data	R_e Stat	M(B) Stat	m* Stat	Const FP	M(B) FP	m* FP
Hydral N3311			131.8	49.13	-23.04	11.39	-17.40	-22.80	11.63
AWM3 N5629			83.2	36.51	-22.34	12.44	-17.14	-22.34	12.25
A262 N708			74.10	35.06	-22.51	12.44	-17.36	-22.41	12.19
A496			51.30	46.43	-23.13	13.23	-1.58	-23.13	13.38
A539 d47			45.71	42.34	-22.86	13.54	-17.45	-22.86	13.56
A2052			40.00	39.80	-23.14	13.42	-17.81	-23.14	13.36
A1139 U6057			30.90	33.18	-22.41	14.32	-17.34	-22.41	13.99
A119			32.40	41.13	-23.08	14.01	-17.70	-23.08	13.99
A85			33.10	46.89	-23.72	13.61	-18.16	-23.72	13.78
A978			30.20	45.12	-23.14	14.30	-17.63	-23.14	14.42
A2255			20.40	43.97	-23.36	14.88	-17.89	-23.36	14.96
A2420			24.50	56.37	-23.41	14.97	-17.58	-23.41	15.41
A1126			18.20	42.12	-23.32	15.07	-17.91	-23.32	15.09
A2440			15.80	39.78	-22.81	15.77	-17.48	-22.81	15.70
A2218			6.69	30.56	-22.33	17.54	-17.38	-22.33	17.09
A2218-L244	207	209	8.51	40.39	-22.66	17.29	-17.31	-22.66	17.25
A665-1150	294	298	11.38	55.64	-23.48	16.54	-17.67	-23.48	16.96
AC103(1)			5.70	44.77	-23.17	17.88	-17.67	-23.17	17.98
AC103(2)			5.73	45.01	-23.30	17.75	-17.80	-23.30	17.86
MS1512+36	290	298	4.76	44.05	-23.18	18.23	-17.70	-23.18	18.31
A370 20	334	343	7.63	70.72	-24.07	17.34	-17.91	-24.07	18.11
CL0024 186	382	393	3.99	38.22	-22.56	18.92	-17.29	-22.56	18.92
CL1447(1)			4.26	40.76	-22.79	18.69	-17.43	-22.79	18.65
CL1447(2)			3.95	37.87	-22.43	19.05	-17.18	-22.43	18.91
CL1447(3)			3.78	36.16	-22.62	18.86	-17.43	-22.62	18.65
CL1447(4)			3.07	29.40	-22.43	19.05	-17.54	-22.43	18.54
Abell 851			3.00	29.80	-22.53	19.03	-17.62	-22.53	18.55
CL0016			3.57	45.31	-23.22	18.87	-17.70	-23.22	18.99
CL1601(2)			3.86	49.21	-23.00	19.10	-17.36	-23.00	19.34
MS1054 1484	330	348	1.88	33.04	-22.46	20.34	-17.40	-22.46	20.01
CL1603-431			1.54	28.54	-22.46	20.46	-17.61	-22.46	19.91
03.1077			1.74	33.49	-22.40	20.59	-17.32	-22.40	20.28
3C324			1.93	44.42	-22.82	20.56	-17.38	-22.82	20.65
53W002*			1.1	39.07					

* Angular Radius only, surface brightness data unreliable.

Table 3C
First-Rank Elliptical Galaxies
Average Parameters Versus Redshift

Galaxy Grouping	# Galaxies	SB(B)	M(B)	R_e
		$z = 0$	Stat	Stat
$z = 0.00$ to 0.177	16	23.69	-22.95	41.8
Standard Deviation		0.24	0.40	6.2
$z = 0.183$ to 1.206	17	23.72	-22.88	40.91
Standard Deviation		0.20	0.46	10.3
All Galaxies	33	23.71	-22.91	41.6
Standard Deviation		0.22	0.43	8.6

Table 3C shows the average values of the surface brightness at zero redshift (SB less $2.5 \log{(1 + z)}$), the effective physical radii and the absolute magnitudes for both low and high z galaxies. These averages show that the three parameters are nearly independent of the redshift. These results confirm that first-rank elliptical galaxies do not evolve with redshift as predicted by the PCP and as hypothesized for the static universe.

9.2   Cluster Elliptical Galaxies — Kochanek

As previously indicated, the cluster elliptical galaxies vary widely in luminosity and physical size. In order to do the surface brightness test, the elliptical galaxies must be referenced to a (arbitrary) standard elliptical galaxy. Fortunately, this can be done using the fundamental plane method. The fundamental plane is based on the empirical observation that the surface brightness, the log of the effective physical radius and the log of the velocity dispersion are closely related by the linear equation

$$SB = -3.76 \log{(\sigma)} + 3.03 \log{(R_e)} + \mathrm{C} \tag{51}$$

where σ is the velocity dispersion, R_e is the effective (half-light) radius and C is a constant.

Kochanek re-analyzed observational data from Jorgensen [36] on local elliptical galaxy clusters assuming an expanding universe with $q = 0.5$ and $H = 50$ km/sec/Mpc and found that C = 26.25 for the F606W band. Using Kochanek's value of C and assuming the static universe model and the F814W band, I found that C = 25.42.

The fundamental plane is applied as follows:

1. R_E is calculated from the effective angular radius, θ, and the normalized distance, r, assuming $H = 50$ Km/sec/Mpc using the equation

$$R_e = 29.09 \; r\theta. \tag{52}$$

2. The velocity dispersion, σ, was measured using an aperture with a physical diameter equivalent to 3.4 arcsec projected on to a galaxy in Coma.

Since the physical diameter so defined depends on the cosmological model at higher z, the physical diameters were converted to equivalent static universe diameters, assuming a $q = 0.5$ expanding universe model was used initially to calculate the diameters. Then, the velocity was normalized to the static universe model using the following equation [34]

$$\log\left(\sigma_{static}\right) = \log\left(\sigma_{exp}\right) + 0.04\ \log\left(\frac{R_{static}}{R_{exp}}\right). \tag{53}$$

As a result, the measured dispersion velocities are larger in the static universe model.

3. Using the static universe parameters of each elliptical galaxy and with the surface brightness reduced to the rest frame $z = 0$ by subtracting $2.5\log\left(1 + z\right)$, the constant C in equation 51 is calculated for each galaxy.

4. Then, assuming a standard elliptical galaxy (with specified values of the parameters), the rest frame surface brightness of each galaxy is calculated from the previously determined values of the constant, C.

5. Finally, the surface brightness of the galaxy in the original redshifted frame is calculated by adding $2.5\log\left(1 + z\right)$ to the rest frame surface brightness.

For the standard elliptical galaxy with $R_e = 10$ Kpc and a velocity dispersion of 225 Km/sec, the regression equation for the surface brightness in the F814W band is

$$SB = 0.98\left[2.5\log\left(1 + z\right)\right] + 19.65. \tag{54}$$

The slope has a standard deviation of only 0.22 magnitudes. This relation is plotted in Figure 6 (left hand panel). It again shows that surface brightness observations fit the static universe model.

However, this result must be considered suspect since the fundamental plane method is circular, i.e., the test will tend to support whatever cosmological model is used to calculate the effective physical radius.

For example, the test shown in Figure 6 (right hand panel) uses effective physical radii calculated assuming an expanding universe with $q = 0.5$. The resulting slope of 2.48 (plus evolutionary brightening) tends to confirm the expanding universe model.

Consequently, the use of only tests based on the fundamental plane method can not be relied upon to decide between the static universe and expanding universe models. However, once the type of universe is determined by other tests not susceptible to the circularity, i.e., the surface brightness test using first-rank elliptical galaxies, the fundamental plane method can be used as a tool to refine the static universe parameters of elliptical galaxies.

Table 4C shows the average values of the surface brightness at zero redshift (surface brightness less $2.5\log\left(1 + z\right)$) and the absolute magnitudes for three ranges of z. Note R_e is fixed at 10 Kpc and the velocity dispersion at 225 km/sec. These averages show that the two parameters are nearly independent of the redshift. This confirms that cluster elliptical galaxies do not evolve with redshift.

38

Surface Brightness for Static Universe
Cluster Elliptical Galaxies
10 Kpc and 225 km/sec Galaxies
Slope 0.98 (.22)
Constant 19.65 (.04)
Std Dev 0.26 mag
Max z 0.83

Surface Brightness F814W Band mag/theta^2

Exp Univ
Theor

Static Univ

Outliers

22

21

20

19

0.0   0.2   0.4   0.6

2.5 log(+ z)

Surface Brightness for Expand Universe
Cluster Elliptical Galaxies
10 Kpc and 225 km/sec Galaxies
Slope 2.48 (.22)
Constant 19.62 (.04)
Std Dev 0.26
Max z 0.83

Surface Brightness F814W Band mag/theta^2

Exp Univ
Theor

Exp Univ
Regr

Outliers

22

21

20

19

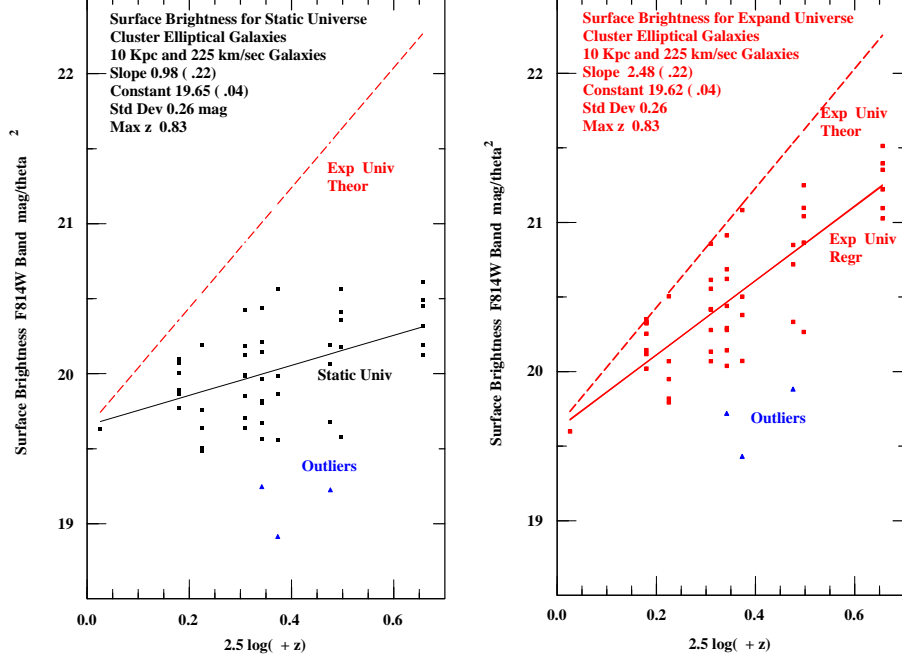0.0   0.2   0.4   0.6

2.5 log(+ z)

Figure 6: Surface brightness of cluster elliptical galaxies. Fundamental plane analysis method used for both graphs. The black line with a slope of 1 represents the theoretical static universe model and the red line is the regression line for the expanding universe observations. The dashed red line represents the theoretical expanding universe models.

Table 4A

Fundamental Plane Analysis of Cluster Elliptical Galaxies

Cluster Data and Corrections

| Cluster	z	r	Abs	K-Corr	Filter Band	Corr to F814W
Local FP	0.024	0.024			F606W	-0.94
A665	0.18	0.166	0.14	0.15	F814W	0.00
A2390	0.23	0.207	0.35	0.20	F814W	0.00
CL 1358+62	0.33	0.285	0.07	0.28	F814W	0.00
A370	0.37	0.315	0.10	0.64	F675W	-0.59
A370	0.37	0.315	0.10	0.32	F814W	0.00
A851	0.41	0.344	0.05	0.56	F702W	-0.47
A851	0.41	0.344	0.05	0.35	F814W	0.00
MS 0015+16	0.55	0.438	0.17	0.51	F814W	0.00
MS 2053-04	0.58	0.457	0.26	0.57	F814W	0.00
MS 1054-03	0.83	0.604	0.07	1.11	F814W	0.00
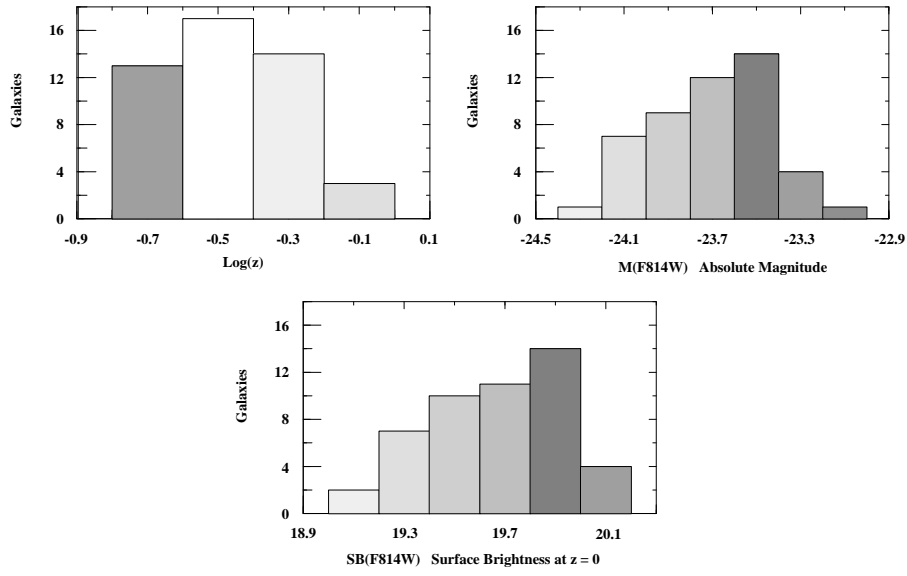
Figure 7: Distribution of static universe parameters of test sample of cluster elliptical galaxies. The parameters were derived from the data using the fundamental plane method and are based on a standard elliptical galaxy with a 10 Kpc radius and a velocity dispersion of 225 Km/s.

Table 4B

Fundamental Plane Analysis of Cluster Elliptical Galaxies

Static Universe Model Parameters

Cluster Galaxy	SB Data	SB Corr	Disp Stat	θ Data	R_e Stat	Const FP	SB FP	M FP	m^* FP
Local FP						25.42	19.63	-23.96	11.81
A665									
3	19.78	19.49	277	2.19	10.53	25.40	19.76	-23.98	16.00
15	19.70	19.41	262	1.51	7.29	25.71	20.07	-23.67	16.31
26	19.28	18.99	228	1.07	5.16	25.52	19.89	-23.86	16.13
42	19.21	18.92	250	1.05	5.04	25.63	20.00	-23.75	16.24
57	18.73	18.44	213	0.66	3.18	25.49	19.86	-23.89	16.10
61	18.93	18.64	230	0.71	3.41	25.73	20.09	-23.65	16.33
77	20.39	20.10	150	1.29	6.20	25.70	20.07	-23.68	16.31
80	19.12	18.83	190	0.66	3.18	25.70	20.06	-23.68	16.31
A2390									
6	19.67	19.12	208	1.02	6.16	25.22	19.63	-24.16	16.31
7	20.16	19.61	191	1.48	8.91	25.09	19.50	-24.29	16.18
9	18.63	18.08	237	0.62	3.71	25.06	19.47	-24.32	16.15
10	19.33	18.78	180	0.60	3.63	25.34	19.75	-24.04	16.43
138	20.87	20.32	108	0.74	4.46	25.77	20.18	-23.61	16.86
CL1358+62									
236	19.69	19.34	168	0.58	4.77	25.34	19.83	-24.04	17.13
256	19.43	19.08	277	0.98	8.11	25.19	19.69	-24.18	16.98
269	19.27	18.92	347	0.83	6.90	25.62	20.11	-23.76	17.40
298	19.31	18.96	284	0.74	6.15	25.48	19.98	-23.90	17.27
375	20.96	20.61	306	2.45	20.36	25.67	20.17	-23.70	17.46
408	19.02	18.67	269	0.40	3.30	25.92	20.41	-23.46	17.70
454	21.08	20.73	173	1.55	12.85	25.48	19.97	-23.90	17.28
470	19.91	19.56	188	0.91	7.57	25.13	19.63	-24.25	16.92
A370									
1	21.51	20.18	336	2.14	19.58	25.42	19.95	-23.96	17.42

Cluster Galaxy	SB Data	SB Corr	Disp Stat	θ Data	R_e Stat	Const FP	SB FP	M FP	m^* FP
2	23.42	22.09	258	8.91	81.62	25.02	19.55	-24.36	17.02
10	21.66	20.33	199	1.41	12.94	25.26	19.79	-24.12	17.26
24	20.51	19.18	255	0.79	7.27	25.27	19.80	-24.11	17.28
28	19.92	19.50	225	0.68	6.19	25.60	20.15	-23.78	17.60
41	19.39	18.97	298	0.51	4.70	25.90	20.42	-23.48	17.90
67	21.05	20.63	164	1.02	9.37	25.67	20.20	-23.71	17.67
77	21.71	20.38	96	0.91	8.35	25.70	19.23	-24.68	16.70
79	20.28	18.95	171	0.46	4.19	25.12	19.65	-24.26	17.13
A851									
23	20.31	19.23	191	0.65	6.45	24.98	19.54	-24.40	17.17
57	19.91	18.83	203	0.41	4.07	25.29	19.84	-24.09	17.48
69	20.43	20.03	197	0.58	5.75	26.99	20.55	-23.39	18.18
102	19.78	18.70	152	0.23	2.34	25.41	19.97	-23.97	17.60
111	21.36	20.28	59	0.55	5.49	24.34	18.90	-25.04	16.53
MS 0015+16									
2	23.84	23.16	264	10.23	130.5	25.38	20.04	-24.00	18.10
7	19.97	19.29	200	0.51	6.54	24.99	19.65	-24.39	17.71
13	19.69	19.01	270	0.41	5.19	25.51	20.17	-23.87	18.23
56	15.68	15.00	222	0.03	0.40	25.54	19.20	-24.84	17.26
MS 2053-04									
197	21.59	20.76	327	1.58	21.09	25.70	20.39	-23.68	18.52
311	20.45	19.62	228	0.38	5.06	25.86	20.54	-23.52	18.67
422	20.05	19.22	135	0.31	4.11	24.87	19.55	-24.51	17.68
432	20.96	20.13	165	0.50	6.67	25.47	20.15	-23.91	18.28
551	19.56	18.73	222	0.22	2.91	25.65	20.33	-23.73	18.46
MS 1054-03									
1294	21.35	20.17	326	0.66	11.61	25.73	20.57	-23.65	19.15
1359	20.39	19.21	232	0.30	5.31	25.25	20.09	-24.13	18.66
1405	21.87	20.69	267	0.95	16.79	25.44	20.28	-23.94	18.86
1457	21.42	20.24	216	0.58	10.12	25.31	20.16	-24.07	18.73
1484	22.24	21.06	340	1.55	27.23	25.57	20.41	-23.81	18.99
1567	21.09	19.91	269	0.47	8.22	25.61	20.46	-23.77	19.03

*For standard elliptical galaxy: $R_e = 10$ Kpc and $\sigma = 225$ km/sec.

Table 4C
Cluster Elliptical Galaxies
Average Parameters Versus Redshift
(10 Kpc and 225 km/sec)

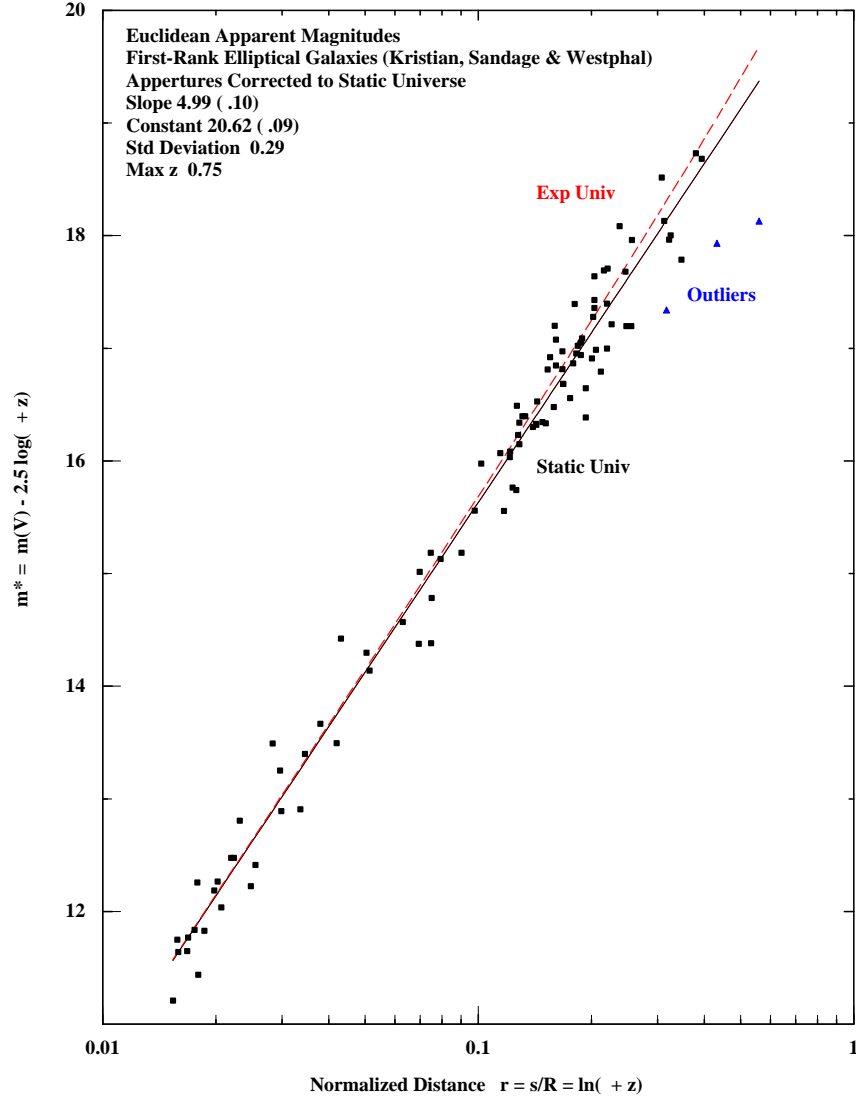| Galaxy Grouping	# Galaxies	SB(F814W) $z = 0$	M(F814W) Stat
$z = 0.00$ to 0.23	14	19.66	-23.91
Standard Deviation		0.23	0.23
$z = 0.33$ to 0.37	15	19.61	-23.96
Standard Deviation		0.29	0.29
$z = 0.41$ to 0.83	18	19.66	-23.91
Standard Deviation		0.28	0.28
All Galaxies (Less 3 outliers)	47	19.64	-23.92
Standard Deviation		0.27	0.27

Figure 8: Euclidean apparent magnitudes of first-rank elliptical galaxies. Black line is the static universe regression line with slope 1. The red dashed line represents the theoretical $q = 0.5$ expanding universe model.

43

10 Euclidean Apparent Magnitude

The observed luminosity, l, of a galaxy in the flat static universe model after K-corrections and corrections for galactic absorptions is given by

$$l = \frac{L}{4\pi s^2 (1 + z)} \tag{55}$$

where L is the absolute luminosity of the galaxy, s is the Euclidean distance and the factor $(1 + z)$ accounts for the loss of energy due to the Hubble redshift.

Then, the equation for the apparent magnitude, m, for the flat static universe model is given by

$$m = M + 5 \log r + 2.5 \log (1 + z) + \mathrm{C} \tag{56}$$

where r is the normalized Euclidean distance, $r = s/(2R) = \ln(1 + z)$. R is the mean interactive radius of the universe, equal to ≈ 8.5 billion light years for a Hubble constant of $H = 59$ km/sec/Mpc. The absolute magnitude, M, is assumed constant since no evolution occurs in the static universe model.

For the expanding universe models, the apparent magnitude, m, is generally plotted versus $\log z$. Instead, the "Euclidean apparent magnitude", defined as

$$m^* = m - 2.5 \log (1 + z) \tag{57}$$

is plotted versus $\log r$. The plot of m^* versus $\log r$ is theoretically linear with a slope of 5 since it represents the inverse square law reduction in luminosity in an Euclidean universe.

The linearity of the plot is the practical reason for plotting m^* rather than m. Then, the data can be analyzed by simple linear regression methods. And, since m^* and m only differ by a function of z which is much more accurately determined than m, the error statistics of $m*$ and m are very nearly the same.

For supernovae, the Euclidean apparent magnitude $m^* = m - 5 \log (1 + z)$. $m*$ is increased by $2.5 \log (1 + z)$ due to time-dilation (see section 6) of the period of the supernovae light curve. This time-dilation accounts for the observed anomalous dimming of type Ia supernovae at high z.

10.1 First-Rank Elliptical Galaxies — Kristian, Sandage & Westphal

Two Hubble diagrams for first-rank elliptical galaxies are shown, one from Kristian, Sandage and Westphal [47] and other derived from the surface brightness and effective angular radii of first-rank elliptical galaxies (many observers).

The Kristian data will be discussed first. The magnitudes for the first-rank elliptical galaxies are corrected based on the cluster Abell richness and Bautz-Morgan contrast classes, the K-correction and galactic absorption.

Figure 8 shows the a plot of the Euclidean apparent magnitude using aperture corrected data for the static universe model as described in the next paragraph. Kristian expected a linear relation between m and $\log(z)$ corresponding

to $q = 1$ but actually found that the slope decreased since the first-rank elliptical galaxies appeared more luminous at higher z. The increased luminosity was attributed to evolution. However, there is another possibility if the static universe model is correct.

This data was observed before the capability to determine the effective radius was possible. Consequently, the apparent magnitudes were measured through a fixed angular aperture and then corrected [48], assuming a $q = 1$ expanding universe model and $H = 50$ km/sec/Mpc, to the standard physical diameter of a first-rank elliptical galaxy. Since the physical diameters for the same angular aperture and z are larger in the $q = 1$ expanding universe model than the static universe model, the apparent magnitudes are less (brighter) than apparent magnitudes in the static universe model. Therefore, before plotting the data, the apparent magnitude data was re-corrected to the standard diameter based on the static universe model. The largest correction was small, only 0.16 magnitudes less bright.

Then, the following regression relation for the static universe was found

$$m^* = 4.99 \log(r) + 20.62 \tag{58}$$

with a standard deviation of 0.10 magnitudes for the slope. Although this data was obtained in the late 1970's, it is an excellent fit to the static universe model.

10.2   First-Rank Elliptical Galaxies — Many Observers

For the second data set on first-rank elliptical galaxies, the apparent magnitude is calculated from the surface brightness and the effective angular radius using the equation

$$m_e = SB - 2.5 \log(\pi \theta^2), \tag{59}$$

where θ is the effective angular radius and

$$m = m_e - 0.75 \tag{60}$$

For the first-rank elliptical galaxies, the regression equation is

$$m^* = 5.14 \log(r) + 21.90. \tag{61}$$

The slope is 5.14 with a standard deviation of 0.16. This is greater than the theoretical slope of 5.0 for a static universe model but is still within one standard deviation of the theoretical slope.

However, it is possible to do much better with this data by using the fundamental plane method. The absolute magnitudes can be referred to a standard first-rank elliptical galaxy using the fundamental plane relation [45]

$$M(B) = -3.33 \log(R_e) + \text{constant.} \tag{62}$$

After carrying through the fundamental plane calculations, the revised regression equation for the first-rank elliptical galaxies is

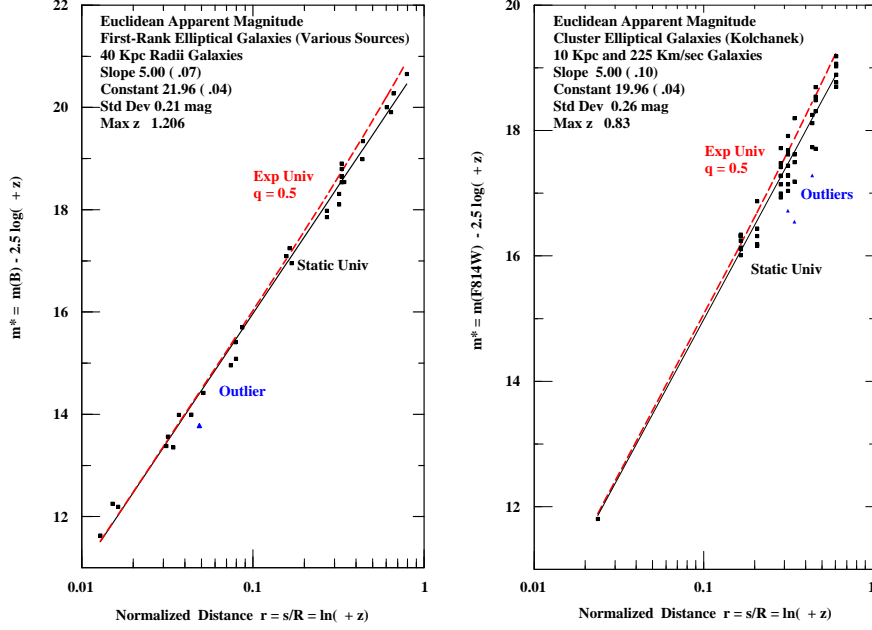$$m^* = 5.00 \log(r) + 21.96. \tag{63}$$

Figure 9: Euclidean apparent magnitudes of first-rank and cluster elliptical galaxies. Both analyzed using the fundamental plane method. Black lines represent the static universe model observations with theoretical slope 5. Red dashed lines represent the expanding universe for $q = 0.5$.

This regression equation represents a first-rank elliptical galaxy with an effective radius of 40 Kpc and is plotted in Figure 9 (left hand panel). The slope now has a standard deviation of only 0.07 magnitudes.

10.3   Cluster Elliptical Galaxies — Kochanek

For the cluster elliptical galaxies, the regression equation is

$$m^* = 5.00 \log{(r)} + 19.96. \tag{64}$$

This regression equation represents the Euclidean apparent magnitude for a standard cluster elliptical galaxy with an effective radius of $R_e = 10$ Kpc and a velocity dispersion $\sigma = 225$ km/sec. Since the standard deviation of the slope is 0.10, the static universe model is verified. The regression equation is plotted in Figure 9 (right hand panel).

Note: The observationally determined slopes for both the first-rank and cluster elliptical galaxies are equal to the theoretical slope of 5 to two decimal
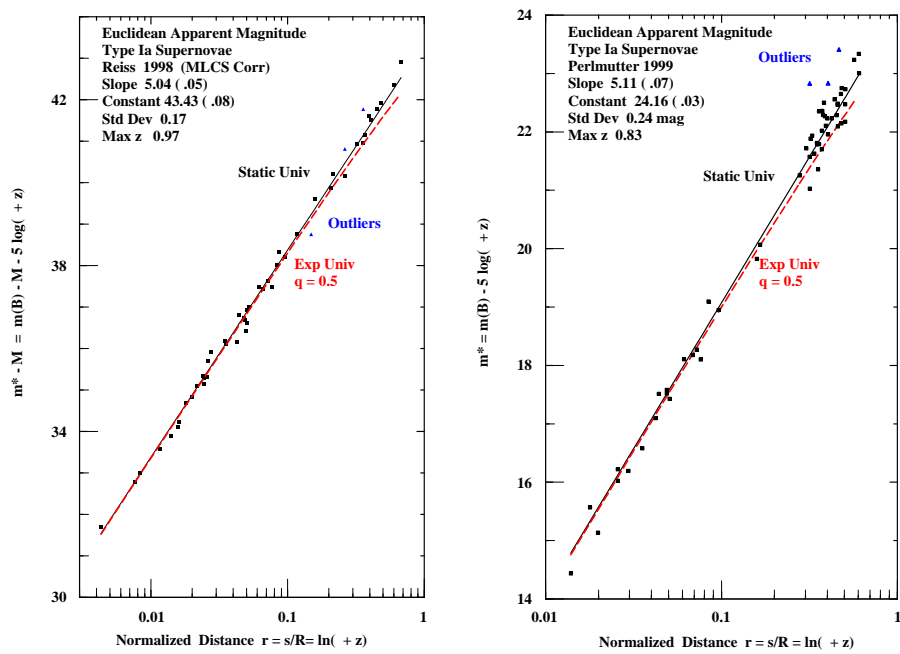
Figure 10: Euclidean apparent magnitude for type Ia supernovae. Black lines with theoretical slope 5.0 represent the static universe model and red dashed lines represent the theoretical $q = 0.5$ expanding universe model.

points. Although this is a coincidence (and quite unlikely), it does attest to the precision of the data and the validity of the static universe hypothesis.

10.4   Type Ia Supernovae — Reiss, Perlmutter

Type Ia supernovae observations have been made by two independent supernovae observation teams. Since for supernovae, $m^* = m - 5\log\left(1+z\right)$ is the appropriate quantity to plot for a linear Hubble relation, the quantity $5\log\left(1+z\right)$ was subtracted from the maximum apparent magnitudes for the supernovae listed in their papers. The supernovae observations are plotted in Figure 10.

The regression equation using the observational data of Reiss [49] is

$$m^* - M = m - M - 5\log\left(1+z\right) = 5.04\log\left(r\right) + 43.43 \tag{65}$$

where M is the absolute magnitude. Since the standard deviation of the slope is only 0.05, this verifies the static universe model.

The regression equation using the data of Perlmutter [50] is

$$m^* = m - 5\log\left(1+z\right) = 5.11\log\left(r\right) + 24.16. \tag{66}$$

In this case, the standard deviation is 0.07, showing that the slope is nearly two standard deviations from the expected slope of 5 for the static universe model.

Both of the above regressions include the effect of time-dilation resulting from the variation of the luminosity of the supernovae over a period of several months or more.

It is important to note that for supernovae, luminosity evolution with z is not expected because the luminosity only depends on the physics of the explosion. This property of supernovae is very useful since it can be used to show indirectly that elliptical galaxies also do not evolve with z.

To show this, first consider that the good fits of the supernovae observations (Figure 10) confirm the static universe model. Then, it follows logically from the good fits of first-rank and cluster elliptical galaxies (Figure 9) to the static universe model that first-rank elliptical galaxies also do not evolve in luminosity with z.

Of course, the non-evolution of elliptical galaxies does appear to contradict current theoretical studies on the evolution of stars which predict that elliptical galaxies are brighter at earlier times. Although it is clear that stars evolve, it may be argued, nevertheless, that other processes exist, for example, the merging of galaxies, that tend to maintain first-rank elliptical galaxies in an equilibrium state.

Analysis of the supernovae plots shows that supernovae become progressively dimmer than expected at high z. However, there is no indication of a comparable dimming of first-rank and cluster elliptical galaxies. (Note that the theoretical $q = 0.5$ expanding universe curve is on opposite sides of the curves for the supernovae and the first-rank and cluster elliptical galaxy plots.) Since light propagates identically in the universe for supernovae and elliptical galaxies, the dimming effect can only be attributed to some feature uniquely associated with
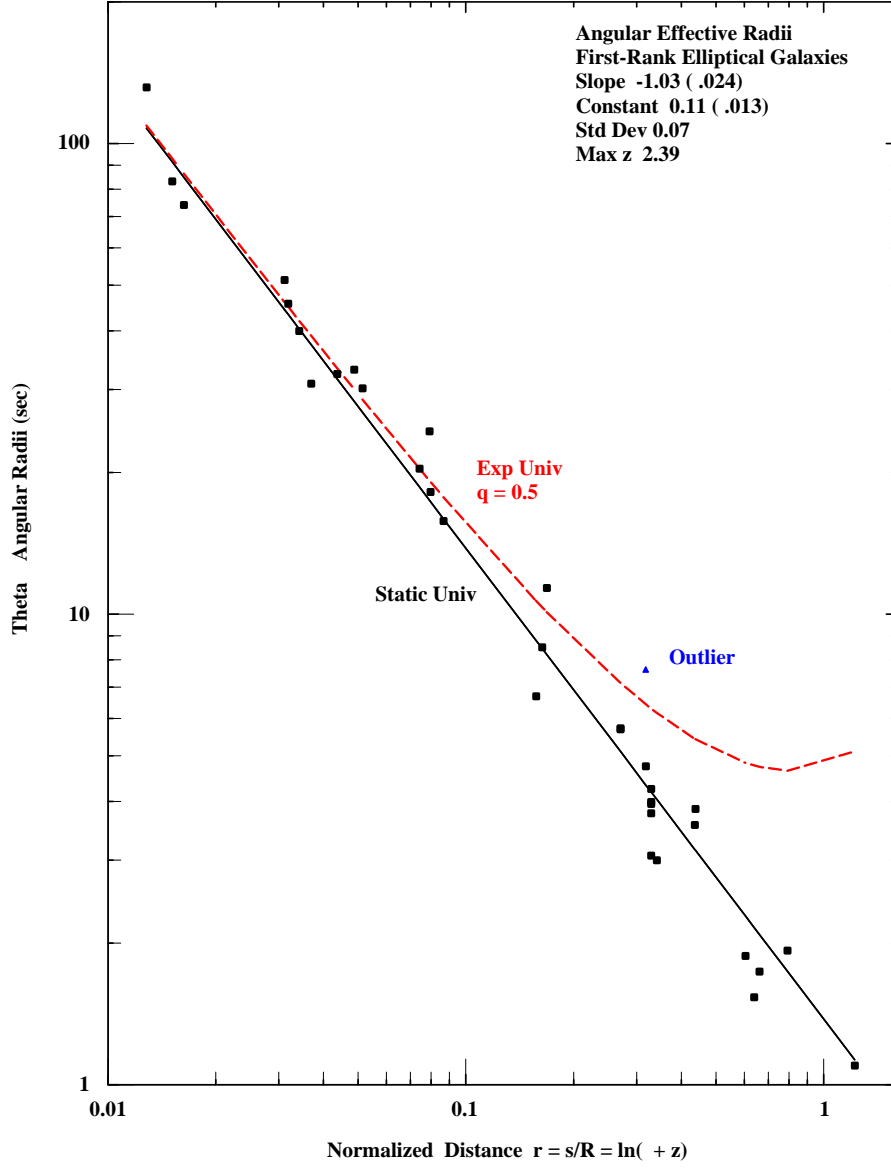
Figure 11: Angular radii of first-rank elliptical galaxies. The black line is the static universe regression line with a slope of -1.03. The red dashed line represents the $q = 0.5$ expanding universe model with constant radii.

supernovae. This is a strong logical argument for supporting time-dilation of the supernovae light curve as the correct explanation of the dimming.

11 Angular Size

For the static universe, the theoretical relation between the effective angular radius, θ, the physical radius, R_E and the normalized distance, $r = ln(1 + z)$, is given by

$$\theta = \frac{R_E}{(29.09 \, r)}. \tag{67}$$

If the logarithm's of the variables in the above relation are plotted, the plot is a straight line with slope -1 assuming R_E is constant. A constant R_E is a critical assumption for first-rank elliptical galaxies but is confirmed by recent high-z velocity dispersion observations by several observers of the high z first-rank elliptical galaxies (see Table 3B). Because high-z and low-z first-rank elliptical galaxies have similar velocity dispersions, they must have similar masses and physical sizes.

11.1 First-Rank Elliptical Galaxies — Many Observers

Angular radii of first-rank elliptical galaxies as shown in Table 3B are plotted in Figure 11. The regression equation is given by

$$\log \theta = -1.03 \log (r) + 0.11. \tag{68}$$

Since the standard deviation of the slope is 0.03, the observations fit the static universe very well. The theoretical expanding universe model, assuming the effective physical radii are constant, is also plotted. Because the difference between the models is so large, the angular size plot strongly supports the static universe model.

This is especially true for the distant radio galaxy observed by Pascarelle [46] at $z = 2.39$. This galaxy was not used for the surface brightness or apparent magnitude tests because the surface brightness and the apparent magnitude could not be reliably determined. However, the angular radius was determined accurately. At the above redshift, the distance of this galaxy is approximately 24 billion light years. The age of this galaxy in the static universe model is much larger than the age of the universe in the expanding universe models.

11.2 Double-Lobes of Radio Galaxies — Nilsson

In the 1970's, it was known that plots of the angular diameters versus redshift of the double lobes of radio galaxies fit the static Euclidean model instead of the expanding universe model. Nevertheless, a way to save the expanding universe model was found. Since the power of the double-lobes at high redshift (calculated assuming an expanding universe) was much greater than at low redshift, it was hypothesized that the physical diameters of the double-lobes

were inversely proportional to the power. With this hypothesis, the data fit the expanding universe model. However, this was actually a completely empirical procedure.

In recent years, lower power double-lobes of radio galaxies were observed at high redshift. Then, it was found that the physical diameters of the double-lobes of radio galaxies were not inversely dependent on the power [52]. This falsified the hypothesized inverse power relation.

Here, we specifically check whether the angular diameter data fit the static universe model. The data for the angular diameters, the redshift and the power of the double-lobes of radio galaxies are from Nilsson [51]. The large variation in the diameters of the double-lobes and the generally greater power of the distant radio galaxies constitute the major problems in the proper analysis of the data. Most of the variations in the angular diameters at a given redshift are assumed due to projection effects. A simulation of the projection effects confirms this assumption.

To check whether the physical diameters may be correlated with the large variation in power, the physical diameters of the double-lobes are plotted versus the power in Figure 12 (left-hand panel). Both the physical diameters and the power were calculated assuming the static universe model. The regression equation between the physical diameters and the power is

$$\log(D) = 0.062 \log(Power) - 0.176 \tag{69}$$

where D represents the physical diameters of the double-lobes in Kpc. The variation with power in the physical diameters is, therefore, small compared to the observed range of physical diameters.

Therefore, before determining the regression between the angular diameters and the distance, the observed $\log(D)$ was corrected as follows: The difference between the average $\log(D)$ (corresponding to 343.7 Kpc) and the $\log(D)$ as calculated from the regression, equation 69, was added to the observed $\log(D)$. Then, $\log(\theta)$ was calculated from the corrected $\log(D)$. The corrected $\log(\theta)$ values were plotted in Figure 12 (right-hand panel). The resulting regression is

$$\log(\theta) = -1.02 \log(r) + 1.05 \tag{70}$$

with a standard deviation of 0.06. This result confirms the static universe model.

12   Galaxy Counts

The counting of galaxies is another way of determining the space-time metric. Theoretically, the number of galaxies, N, brighter than apparent magnitude, m, increase as

$$\log(N) = 0.6 \, m + \text{constant} \tag{71}$$

where N is the cumulative number of galaxies observed to apparent magnitude m. This relation holds to about $m = 17$ and then the slope starts to decrease because the K-corrections begins to decrease the number of galaxies that are
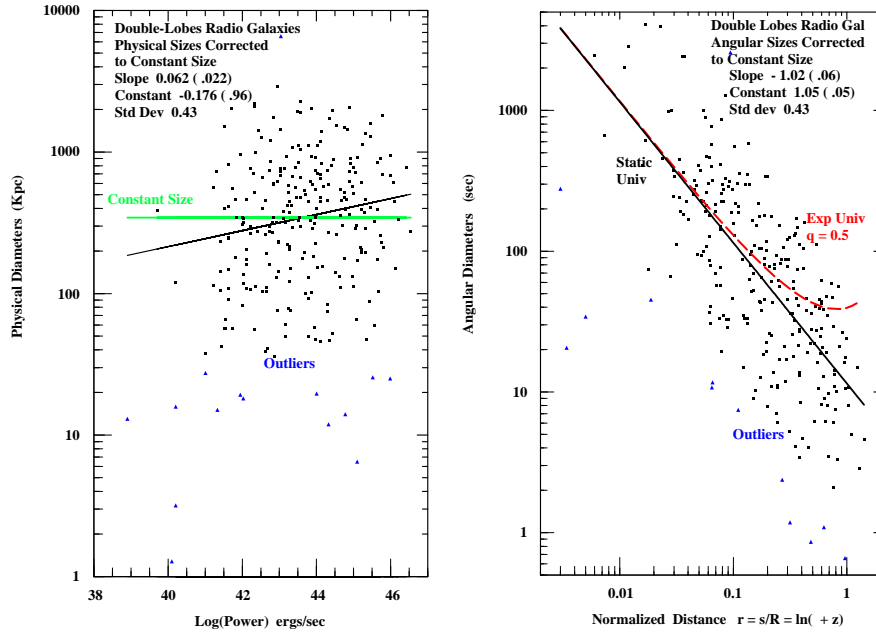
51

Figure 12: Physical and angular radii of double lobes of radio galaxies. Physical diameters are corrected to a constant size and used to correct the angular diameters. The green line represents the corrected constant diameters. The black lines represent the static universe and the dashed red line the $q = 0.5$ expanding universe model.

Table 5A

2dF Survey Schecter Luminosity Functions
for $H = 100$ km/sec

Galaxy Type	$M(b_j)^*$	α	ϕ^* (10^{-3})
E/SO	-19.61	-0.74	9.0
Sab	-19.68	-0.86	3.9
Sbc	-19.38	-0.99	5.3
Scd	-19.00	-1.21	6.5
Sm/Im	-19.02	-1.73	2.1

visible within a given apparent magnitude range. In the last 20 years, counts of galaxies have been made to approximately $m = 28$ and compared to calculated counts assuming various expanding universe models. It has been generally found that the calculated galaxy counts are considerably less than the observed counts at $m > 20$ unless evolutionary effects are assumed.

More recently, enough redshifts of galaxies have been obtained to make a start on relating galaxy counts to redshifts.

12.1 Counts versus Apparent Magnitude — Tyson

Differential galaxy counts versus apparent magnitude were calculated for both the static universe and the $q = 0.5$ expanding universe model. The calculations were based on the 2dF Survey Schecter luminosity functions [53] as shown in Table 5A. No evolution was assumed in the calculations in either the luminosity or in the space density of the galaxy types.

The 2dF Survey determined the Schecter luminosity functions for five types of galaxies — E/SO, Sab, Sbc, Scd and Sm-Im. For each type of galaxy, K-corrections from King [54] were used to $z = 1.5$. Beyond $z = 1.5$, the K-corrections for E/SO and S_{ab} galaxies were assumed to increase as $1.25 \log{(1 + z)}$. For the other type galaxies, the K-corrections were assumed to remain constant for $z > 1.5$. These K-corrections beyond $z = 1.5$ reflect increases in luminosity from the ultra-violet moving into the b_j band.

The observations are valid to $z = 4$ where the Lyman break (a steep reduction in luminosity at 912 angstroms) corresponds to the center of the observed b_j band at 4500 angstroms. To simulate the Lyman break, the calculated counts were cutoff at $z = 4$. The calculated counts were also cutoff at absolute magnitude -11.0, a reasonable lower limit for the luminosity of galaxies. Galactic extinction was set equal to zero.

The calculations were made using 1/4 magnitude increments over the range 12 to 28.5 magnitudes. It must be said that this required six very large spreadsheets, one for each type of galaxy. On the other hand, using a spreadsheet makes it very easy to determine galaxy counts for each type of galaxy and galaxy counts versus redshift.
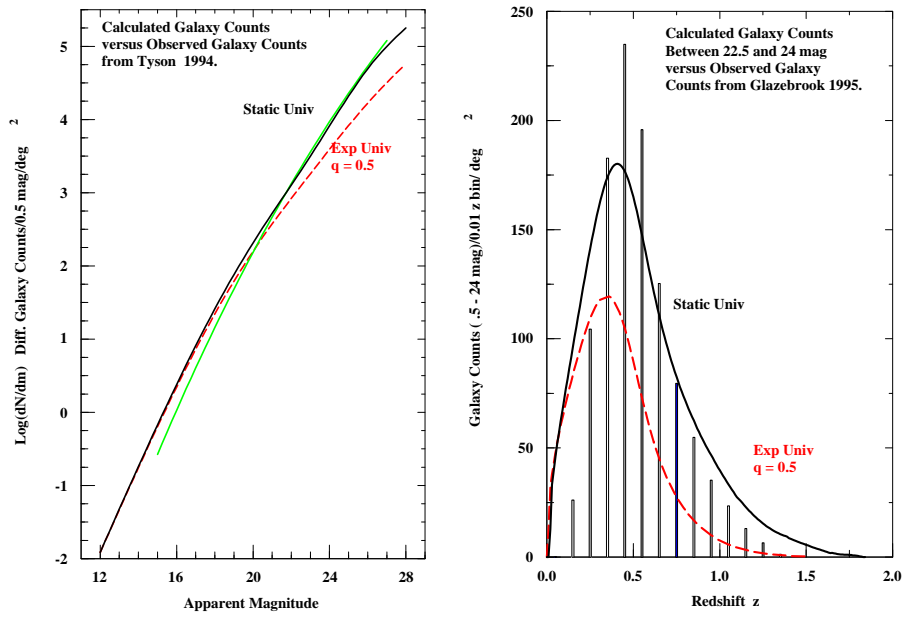
Figure 13: The calculated counts for the static universe and the $q = 0.5$ expanding universe are shown by the black line and the dashed red line, respectively. The green line shows the observed counts by Tyson between 15 and 27 mag. In the right-hand panel, observed counts versus redshift are shown as narrow black bars of width 0.01 in z.

54

The calculated and observed differential galaxy counts are plotted in Figure 13 (left hand panel). The observed differential galaxy counts from Tyson [55] are represented by the green line, valid between $m = 15$ and 27 in the b_j band. However, note that to $m = 20$, the observed counts are less than the calculated counts since Tyson initially picked out areas of sky apparently devoid of galaxies to roughly $m = 19$. But, from $m = 20$ to 27 magnitudes, the observed and calculated counts for the static universe are equal.

On the other hand, the calculated differential galaxy counts based on the expanding universe model with $q = 0.5$ with no evolution are significantly less than the observed counts.

Since the differential galaxy counts in the static universe model are very closely the same as the observed galaxy counts, this is good evidence that medium and high redshift galaxies have the same luminosity distribution and space density as local galaxies. Consequently, the observations both confirm the static universe model and the PCP hypothesis of an equilibrium (no evolution) universe.

12.2   Counts versus Redshift — Glazebrook

Figure 13 (right hand panel) shows the calculated number of galaxies within the apparent magnitude range $22.5 < m < 24.0$ for the static and expanding universe models versus the observed number of galaxies (scaled to a square degree) in redshift bins 0.01 z wide. The observed counts are from Glazebrook [56]. Glazebrook observed 73 galaxies in a 73% complete sample within 7 separate regions with a total angular area of 38.01 sq. arcmin. To compare the observed counts with the calculated counts, the number of counts in Glazebrook's paper were multiplied by a scale factor of 13.05 to conform to the same scale as the calculated counts. The scale factor also accounts for the sample's 73% completeness assuming that the additional galaxies with no measured redshifts have the same redshift distribution. A reasonable agreement with the static universe calculations is observed, again confirming the static universe model.

Since both sets of observations agree with the calculated counts, it was thought useful to also show calculated cumulative galaxy counts by galaxy type to apparent magnitudes 24 and 28 for the range of redshifts from $z = 0.25$ to $z = 4$. These cumulative counts are shown in Tables 5B and 5C. The analysis of the data in the tables shows several important features: First, few if any E/SO galaxies can be observed at $m < 24$ beyond $z = 0.75$. Other type galaxies can be observed to, at most, $z = 1.5$. For $m < 28$, most E/SO galaxies can be observed only to approximately $z = 2$. Very few can be observed to $z = 3$ or $z = 4$. Second, the large numbers of "blue" galaxies at high redshift appear to be Sm-Im. These exist in approximately the number observed by Tyson at $m > 27$.

Table 5B

Cumulative Galaxy Counts to Apparent Magnitude 24
(Logarithm of Galaxy Counts Shown Below)

z	0.25	0.50	0.75	1.0	1.5	2.0	3.0
r	0.22	0.41	0.56	0.69	0.92	0.92	1.10
E/SO	2.76	3.29	3.38	3.38	3.38	3.38	3.38
Sab	2.52	3.08	3.28	3.35	3.38	3.38	3.38
Sbc	2.52	3.11	3.33	3.44	3.52	3.53	3.53
Scd	3.00	3.43	3.56	3.61	3.64	3.65	3.65
Sm-Im	3.23	3.49	3.59	3.63	3.67	3.68	3.68
Totals	3.60	4.01	4.14	4.20	4.23	4.24	4.24

Table 5C

Cumulative Galaxy Counts to Apparent Magnitude 28
(Logarithm of Galaxy Counts Shown Below)

z	0.25	0.50	0.75	1.0	1.5	2.0	3.0	4.0
r	0.22	0.41	0.56	0.69	0.92	1.10	1.39	1.61
E/SO	2.91	3.62	3.96	4.13	4.28	4.33	4.36	4.37
Sab	2.71	3.42	3.77	4.00	4.27	4.42	4.59	4.68
Sbc	2.71	3.43	3.79	4.03	4.32	4.49	4.70	4.81
Scd	3.53	4.11	4.39	4.57	4.73	4.93	5.07	5.14
Sm-Im	4.25	4.60	4.91	4.87	5.01	5.09	5.17	5.20
Totals	4.36	4.79	5.10	5.16	5.33	5.46	5.58	5.64

13　Summary

Because the static universe hypothesis is a simple and logical deduction from the PCP and the observational data amply confirms the deductions of the static universe hypothesis, I conclude that the universe is static and in an equilibrium state. I also find that the new gravitational theory is confirmed by the cosmological observations.

14　Acknowledgments

References

[1] T. Jaakkola (1993), "Equilibrium Cosmology", Progress in New Cosmologies: Beyond the Big-Bang, ed. H.C. Arp, C.R. Keys & K. Rudnicki, Plenum Press, New York, 111.

[2] P.A. LaViolette (1986), Is the Universe Really Expanding?, ApJ 301, 544.

[3] T.B. Andrews (1994), "Theoretical Basis for a Non-Expanding Universe," Frontiers of Fundamental Physics, ed. M. Barone & F. Selleri, Plenum Press, New York, 90.

[4] A. Sandage & L. Lubin (2001), The Tolman Surface Brightness Test for the Reality of the Expansion: I. Calibration of the Necessary Local Parameters, ApJ 121, 2271; II. The Effect of the Point-Spread Function and Galaxy Ellipticity on the Derived Photometric Parameters, ApJ 121, 2289; III. HST Profile and Surface Brightness Data for Early-Type Galaxies in Three High-Redshift Clusters, preprint (astro-ph/0106563); IV. A Measurement of the Tolman Signal and the Luminosity Evolution of Early-Type Galaxies, preprint (astro-ph/0106566).

[5] M. Moles et al. (1998), On the Use of Scaling Relations for the Tolman Test, preprint (astro-ph/9802131), (See section 3).

[6] A. Romer (1973), How to Choose a Theory: Science for Nonscientists, Amer J Phys, 41, 947.

[7] H. Bondi & T. Gold (1948), The Steady-State Theory of the Expanding Universe, MNRAS 108, 252.

[8] F. Hoyle (1948), A New Model for the Expanding Universe, MNRAS 108, 372.

[9] D.A. Varshalovich, A. Y. Potekhin & A.V. Ivanchik (2000), Testing Cosmological Variability of the Fundamental Constants, preprint (ph/0004062).

[10] T.B. Andrews (1997), Derivation of the Schrödinger Equation, "The Present Status of the Quantum Theory of Light," Kluwer Academic Publishers, ed. S. Jeffers, S. Roy, J-P. Vigier & G. Hunter, The Netherlands, 181.

[11] H. Giorgi (1990), An Overview of Symmetry Groups in Physics, Talk presented at 1990 fall meeting of the New England Section of the American Physical Society at Yale University, Harvard preprint number HUTP-90/A065. Also H. Giorgi (1993) "The Physics of Waves", Prentice Hall, Inc., Englewood Cliffs, N.J.

[12] C. Vassallo (1978), Translational Invariance of Wave Guides and Normal Modes, Amer J Phys 46, 1022.

[13] F.Y. Chen (1970), Similarity Transformations and the Eigenvalue Problem of Certain Far-Coupled Systems, Amer J Phys 38, 1036.

[14] T.B. Andrews (1998), Derivation of Newton's Law of Gravitation and Discovery of the Unique Normal Modes of the Universe, "Causality and Locality in Modern Physics," ed. G. Hunter, S. Jeffers & J-P. Vigier, Kluwer Academic Publishers, The Netherlands, 135.

[15] C.A. Croxton (1974), "Introductory Eigenphysics, An Approach to the Theory of Fields," John Wiley & Sons, pp. 142–145.

[16] P.M. Morse & H. Feshbach (1953), "Methods of Theoretical Physics," McGraw-Hill Book Company, Inc., 739.

[17] Q. Wang et al. (2000), "Precise Measurement of Gravity Variations During a Total Solar Eclipse," Physical Review D, 62, 041101(R).

[18] C.S. Unnikrishnan, A.K. Mohapatra & G.T. Gillies (2001), Anomalous Gravity Data During the 1997 Total Solar Eclipse Do Not Support the Hypothesis of Gravity Shielding, Phys Rev D, 63 062002-1.

[19] Nasa (2000), Table 2, Shadow Contacts and Circumstances, Total Solar Eclipse of 1997 March 9, http://umbra.nascom.nasa.gov/eclipse /970309/tables/table2.html.

[20] S. Carlip (1999), Aberation and the Speed of Gravity, preprint (gr-qc/9909087).

[21] G.S.M. Moore (1990), Fractal Gases of Zero Momentum with Respect to All Inertial Frames, Amer J Phys, 58, 581.

[22] R. Furth (1964), A New Hypothesis to Account for the Red-Shift in the Spectra of Distant Stars, Physics Letters, 13, Number 3, 221.

[23] J.D. Anderson et al. (1998), Indications, from Pioneer 10/11, Galileo and Ulysses Data of an Apparent Anomalous, Weak, Long-Range Acceleration, Phys Rev Letters 83, 2858.

[24] G.A. Tammamm & Reindl (1999), The Luminosity Calibration of Sne Ia: Present Status, preprint (astro-ph/9903220).

[25] J.D. Anderson et al. (2001), Un-Prosaic Exposition of a Prosaic Explanation, preprint (gr-qc/0107022).

[26] L.K. Scheffer (2001), Conventional Forces Can Explain the Anomalous Acceleration of Pioneer 10, preprint (gr-qc/0107092).

[27] G. Goldhaber et al. (1996), Observation of Cosmic Time Dilation using Type Ia Supernovae as Clocks, preprint (astro-ph/9602124). Also, G. Goldhaber et al., (2001), Timescale Stretch Parameterization of Type Ia Supernova B-band Light Curves, preprint (astro-ph/0104382)

[28] P.D. Noerdlinger (1966), The Time Dilation of Luminosity Fluctuations of Massive Objects, ApJ 143, 1004.

[29] F. Hoyle et al. (1994), Astrophysical Deductions from the Quasi-Steady State Cosmology, MNRAS 267, 1007.

[30] G. Burbidge (2001), Quasi-Steady State Cosmology, preprint (astro-ph/0108051).

[31] T. Totani et al. (2001), Diffuse Extragalactic Background Light Versus Deep Galaxy Counts in the Subaru Deep Field: Missing Light in the Universe?, ApJ 550:L137.

[32] A. Sandage (1995), "Practical Cosmology: Inventing the Past, The Deep Universe," Edited by B. Binggeli & R. Buser, Saas-Fee Advanced Course 23, Springer-Verlag, 1995, page 12 and chapters 3-6.

[33] C.S. Kochanek et al. (2000), Fundamental Plane of Gravitational Lens Galaxies and the Evolution of Early-Type Galaxies in Low-Density Environments, ApJ 543, 131.

[34] I. Jorgensen et al. (1995), Spectroscopy for E and SO Galaxies in Nine Clusters, MNRAS 276, 1341.

[35] M. Fukugita et al. (1995), Galaxy Colors in Various Photometric Band Systems, PASP 107, 945.

[36] I. Jorgensen et al. (1995), Multicolour CCD Surface Photometry for E and SO Galaxies in 10 Clusters, MNRAS 273, 1097.

[37] A. Sandage & J.M. Perelmuter (1991), The Surface Brightness Test for the Expansion of the Universe. 3. Reduction of Data for the Several Brightest Galaxies in Clusters to Standard Conditions and a First Indication that the Expansion is Real, ApJ 370, 455.

[38] A. J. Barger et al. (1998), New Constraints on the Luminosity Evolution of Spheroidal Galaxies in Distant Clusters, ApJ 501, 522.

[39] I. Jorgensen et al. (1999), The Evolution of Cluster E and SO Galaxies Measured from the Fundamental Plane, preprint (astro-ph/9905155).

[40] R. Bender et al. (1998), Exploring Cluster Elliptical Galaxies as Cosmological Standard Rods, ApJ 493, 529.

[41] P.G. van Dokkum & M. Franx (1996), The Fundamental Plane in CL0024 at $z = 0.4$: Implications for the Evolution of the Mass-to-Light ratio, MNRAS 281, 985.

[42] M. Dickinson (1996), "Cluster Ellipticals at High Redshift: The View from the Ground and with HST", Fresh Views of Elliptical Galaxies, ed. A. Buzzoni, A. Renzini & A. Serrano, ASP Conference Series, Vol. 86, 283.

[43] D. Schade, L.F. Barrientos & O. Lopez-Cruz (1997), Evolution of Cluster Ellipticals from $z = 0.2$ to $z = 1.2$ from HST Imaging, ApJ, 477, L17.

[44] P.G. van Dokkum et al. (1998), Luminosity Evolution of Early-Type Galaxies to z = 0.83: Constraints on Formation Epoch and Omega, ApJ 504, L17.

[45] D. Schade et al. (1999), Hubble Space Telescope Imaging of the CFRS and LDSS Redshift Surveys - 3. Field Elliptical Galaxies at $0.2 < z < 1.0$, preprint (astro-ph/9906171).

[46] Pascarelle et al. (1996), S.M. Pascarelle, R.A Windhorst, S.P. Driver & E.J. Ostrander, The Serendipitous Discovery of a Group or Cluster of Young Galaxies at $z = 2.40$ in Deep Hubble Space Telescope WFPC2 Images, ApJ, 456, L21

[47] J. Kristian, A.R. Sandage & J.A. Westphal, (1978), The Extension of the Hubble Diagram. 2. New Redshifts and Photometry of Very Distant Galaxy Clusters: First Indication of a Deviation of the Hubble Diagram from a Straight Line, ApJ, 221, 383.

[48] A. Sandage, The Redshift-Distance Relation. 1. Angular Diameter of First-Ranked Cluster Galaxies as a Function of Redshift: The Aperture Correction to Magnitudes, ApJ 173, 485.

[49] A.G. Riess et al. (1998), Observational Evidence from Supernovae for an Accelerating Universe and a Cosmological Constant, AJ 116, 1009.

[50] S. Perlmutter et al. (1999), Measurements of Ω and Λ from 42 High-Redshift Supernovae, ApJ 517,, 565.

[51] M.J. Nilsson et al. (1993), On the Redshift Apparent-Size Diagram of Double Radio Sources, ApJ 413, 453.

[52] K.M. Blundell, S. Rawlings & C.J. Willott (1998), Nature and Evolution of Classical Double Radio Sources from Complete Samples, preprint (astro-ph/9810197)

[53] S. Folkes et al. (1999), The 2dF Galaxy Redshift Survey: Spectral Types and Luminosity Functions, preprint (astro-ph/9903456).

[54] C.R. King & R.S. Ellis (1985), The Evolution of Spiral Galaxies and Uncertanties in Interpreting Galaxy Counts, AJ 288, 456.

[55] J.A. Tyson (1994), Optical Extragalactic Background Radiation, "Extragalactic Background Radiation," ed. M. Livio, Cambridge University Press.

[56] Glazebrook et al. (1995), A Faint Galaxy Redshift Survey to $B = 24$, MNRAS, 273, 157.

15   List of Figures

16   Appendix — Simulation of Hubble Redshift

This is the basic program I used to calculate the change in energy due to moving a mass particle or a photon a short distance, s, in the universe.

```
'File Redshift.BAS (Written in MS-DOS QBasic)
'Hubble Redshift Simulation for a Photon or Mass Particle).

'Problem Description:
'To simulate the interaction energy of a particle with all the
'particles in the universe before and after moving the particle
'a small distance, s, to the right along the $x$-axis.

'The Particle's initial position is denoted by Pos1. The final
'position, is denoted by Pos2. Energy inputs from particles
'originate in regions RA, RB and RC. The interaction is of the
'form exp(-r1)/r1 for the particle in position 1 and
'exp(-r2)/r2 for region A, position 2 and exp(-r3)/r3 for
'region C, position 2.

'In RA1, the particle distance is r1 = SQR(x^2 + y^2 + z^2) away
'from particles in the left hand quadrant. Normalized, the effect
'is one-half of the interaction with all the particles in the
'universe.

'In RA2, the moved particle is further away from the particles on
'the left in the universe. Then, r2 = SQR((x + s)^2 + y^2 + z^2).

'In RC2, the moved particle is closer to the particles on the
'right in the universe. Then, r3 = SQR((x - s)^2 + y^2 = z^2).

'The integrations are limited to equal or less than maxs!.

'Results are written to the file "Results.BAS".


'Begin Program

OPEN "RESULTS.BAS" for OUTPUT as #1

'Set Parameters
progi% = 352    'Program Iterations
maxs! = 7.0     'Maximum Radius
ints! = 0.02    'Integration Step
intn% = 3       'Number of Integr Steps Particle Moved to Right
```

```
s! = intn%*ints!              'Distance Particle Moved
pi! = 3.1415926
c! = 4/(4*pi!)*ints!^3      'For Half-Sphere Normalization,
'results correspond to interactions with particles in half
'the universe.

'Initializations
ERA1# = 0
ERA2# = 0
ERB1# = 0
ERC1# = 0

'Main Program

PRINT "REDSHIFT.BAS:  "; "Energy Absorption of a Particle"
PRINT "                "; "at Two Positions, P1 and P2."
PRINT " "
FOR i% = 0 TO progi%
  x! = i% * ints!

  FOR j% = 0 TO progi%
    y! = j% * ints!

    FOR k% = 0 TO progi%
      z! = k% * ints!

      Temp! = y!^2 + z!^2
      r1# = SQR(x!^2 + Temp!)         'Dist for Particle 1A
      r2# = SQR((x! + s!)^2 + Temp!) 'Dist for Particle 2A
      r3# = SQR((x! - s!)^2 + Temp!) 'Dist for particle 2C
      IF r1# = 0 THEN r1# = 20
      IF r3# = 0 THEN r3# = 20

'Region A for Particle 1
      IF r1# <= maxs! THEN                    'Sum to Max Radius
      ERA1# = ERA1# + EXP(-r1#)/r1#
      IF i% = 0 THEN ERA1# = ERA1# - EXP(-r1#)/(2*r1#)
      IF j% = 0 THEN ERA1# = ERA1# - EXP(-r1#)/(2*r1#)
      IF k% = 0 THEN ERA1# = ERA1# - EXP(-r1#)/(2*r1#)
      END IF

'Region A for Particle 2
      IF r2# <= maxs! THEN                    'Sum to Max Radius
      IF i% >= intn% THEN
         ERA2# = ERA2# + EXP(-r2#)/r2#
         IF i% = intn% THEN ERA2# = ERA2# - EXP(-r2#)/(2*r2#)
```

```
            IF j% = 0 THEN ERA2# = ERA2# - EXP(-r2#)/(2*r2#)
            IF k% = 0 THEN ERA2# = ERA2# - EXP(-r2#)/(2*r2#)
         END IF
         END IF


 'Region B for Particle 1 (Same Result for Particle 2)
         IF r1# <= maxs! THEN                'Sum to max radius
         IF i% <= intn% THEN
           ERB1# = ERB1# + EXP(-r1#)/r1#
           IF i% = 0 THEN ERB1# = ERB1# - EXP(-r1#)/(2*r1#)
           IF i% = intn% THEN ERB1# = ERB1# - EXP(-r1#)/(2*r1#)
           IF j% = 0 THEN ERB1# = ERB1# - EXP(-r1#)/(2*r1#)
           IF k% = 0 THEN ERB1# = ERB1# - EXP(-r1#)/(2*r1#)
         END IF
         END IF


 'Region C for Particle 2
         IF r3# <= maxs! THEN                'Sum to Max Radius
         IF i% >= intn% THEN
            ERC1# = ERC1# + EXP(-r3#)/r3#
            IF i% = intn% THEN ERC1# = ERC1# - EXP(-r3#)/(2*r3#)
            IF j% = 0 THEN ERC1# = ERC1# - EXP(-r3#)/(2*r3#)
            IF k% = 0 THEN ERC1# = ERC1# - EXP(-r3#)/(2*r3#)
         END IF
         END IF


 'Output to Screen
         prcheck% = INT(SQR((maxr#^2/2)))
         IF J% = prcheck%  and k% = prcheck% THEN
         ERA1! = ERA1#*c!
         ERA2! = ERA2#*c!
         ERB1! = ERB1#*c!
         ERC1! = ERC1#*c!
         DiffA1A2! = ERA1! - ERA2!
         DiffA1C1! = ERA1! - ERC1!
         PRINT x!; ERA1!; ERA2!; ERB1!; ERC1!; DiffA1A2!; DiffA1C1!
         END IF

         NEXT k%
      NEXT j%
  NEXT i%

 'Output to File
 ERA1! = ERA1#*c!
 ERA2! = ERA2#*c!
 ERB1! = ERB1#*c!
```

```
ERC1! = ERC1#*c!
DiffA1A2! = ERA1! - ERA2!
DiffA1C1! = ERA1! - ERC1!
Print #1, " "
Print #1, "Program REDSHIFT.BAS:    "; "Energy Absorption of Particle"
Print #1, " "
Print #1, "Parameters: ";
Print #1, " "
Print #1, "Program Iterations (progi%) = "; progi%
Print #1, "Maximum Radius (maxr#)      = "; maxs!
Print #1, "Integration Step (ints!)    = "; ints!
Print #1, "Particle Steps (intn%)      = "; intn%
Print #1, " "
Print #1, "Particle Position (s!)      = "; s!
Print #1, " "
Print #1, "Results"
Print #1, " "
Print #1, "EnergyRA1 (ERA1#) =: "; ERA1!
Print #1, "EnergyRA2 (ERA2#) =: "; ERA2!
Print #1, "EnergyRB1 (ERB1#) =: "; ERB1!
Print #1, "EnergyRC1 (ERC1#) =: "; ERC1!
Print #1, " "
Print #1, "Difference A1A2 (DiffA1A2#) = "; DiffA1A2!
Print #1, "Difference A1C1 (DiffA1C1#) = "; DiffA1C1!
Print #1, " "
Print #1, "End Results"

CLOSE #1
END


The output of the program for one set of parameters is
shown below: The main result is Diff A1A2 = 0.00987
which should equal (s/R)E = 0.01E.


Program REDSHIFT.BAS:  Energy Absorption of Particle


Parameters:
Program Iterations (progi%) =  1002
Maximum Radius (maxr#)      =  10
Integration Step (ints!)    =  0.01
Particle Steps (intn%)      =  1

Particle Position (s!)      =  0.01

Results
```

```
EnergyRA1 (ERA1#) =:   .499629
EnergyRA2 (ERA2#) =:   .4897593
EnergyRB1 (ERB1#) =:   4.799089E-3
EnergyRC1 (ERC1#) =:   .499629

Difference A1A2 (DiffA1A2#) =  9.869665E-3
Difference A1C1 (DiffA1C1#) =  0

End Results
```